# Cohort-mean measured macromolecules lead to more robust linear-combination modeling than parameterized and subject-specific ones

Helge J. Zöllner[1,2,*], Christopher W. Davies-Jenkins[1,2], Saipavitra Murali-Manohar[1,2], Tao Gong[3,4], Steve C. N. Hui[1,2], Yulu Song[1,2], Weibo Chen[5], Guangbin Wang[3,4], Richard A. E. Edden[1,2], Georg Oeltzschner[1,2]

*[1] Russell H. Morgan Department of Radiology and Radiological Science, The Johns Hopkins University School of Medicine, Baltimore, MD, United States*
*[2] F. M. Kirby Research Center for Functional Brain Imaging, Kennedy Krieger Institute, Baltimore, MD, United States*
*[3]Departments of Radiology, Shandong Provincial Hospital Affiliated to Shandong First Medical University, Jinan, Shandong, 250021,China*
*[4]Departments of Radiology, Shandong Provincial Hospital, Cheeloo College of Medicine, Jinan, Shandong, 250021,China*
*[5]Philips Healthcare, Shanghai, China*

***Corresponding author:**

Helge Jörn Zöllner, Ph.D.

Division of Neuroradiology, Park 365

The Johns Hopkins University School of Medicine

600 N Wolfe St

Baltimore, MD 21287

hzoelln2@jhmi.edu

*Word count: 7343*

*Figure count: 7*

*Key words: Linear-combination modeling, short-TE MRS, macromolecules, aging*

*Abbreviations: linear-combination modelling – LCM, macromolecular – MM, Akaike information criterion – AIC, measured MM – mMM, parameterized MM – pMM, posterior cingulate cortex – PCC, full-width half-maximum – FWHM, Hankel singular value decomposition – HSVD, total macromolecules – tMM, linear mixed-effect model – LME, Inter-class correlation coefficients – ICC, spline baseline – spbl.*

# Abstract

Expert consensus recommends linear-combination modeling (LCM) of $^{1}$H MR spectra with sequence-specific simulated metabolite basis function and experimentally derived macromolecular (MM) basis functions. Measured MM basis functions have been derived from metabolite-nulled spectra averaged across a small cohort. The use of subject-specific instead of cohort-averaged measured MM basis functions has not been studied. Furthermore, measured MM basis functions are not widely available to non-expert users, who commonly rely on parameterized MM signals internally simulated by LCM software. To investigate the impact of the choice of MM modeling, this study, therefore, compares metabolite level estimates between different MM modeling strategies (cohort-mean measured; subject-specific measured; parameterized) in a lifespan cohort and characterizes its impact on metabolite-age associations.

100 conventional (TE = 30 ms) and metabolite-nulled (TI = 650 ms) PRESS datasets, acquired from the medial parietal lobe in a lifespan cohort (20-70 years of age), were analyzed in Osprey. Short-TE spectra were modeled in Osprey using six different strategies to consider the macromolecular baseline. Fully tissue- and relaxation-corrected metabolite levels were compared between MM strategies. Model performance was evaluated by model residuals, the Akaike information criterion (AIC), and the impact on metabolite-age associations.

The choice of MM strategy had a significant impact on the mean metabolite level estimates and no major impact on variance. Correlation analysis revealed moderate-to-strong agreement between different MM strategies ($r > 0.6$). The lowest relative model residuals and AIC values were found for the cohort-mean measured MM. Metabolite-age associations were consistently found for two major singlet signals (tCr, tCho) for all MM strategies, however, findings for highly J-coupled metabolites it was depended on the MM strategy. A variance partition analysis indicated that up to 44% of the total variance was related to the choice of MM strategy. Additionally, the variance partition analysis reproduced the metabolite-age association for tCr and tCho found in the simpler correlation analysis.

In summary, the inclusion of a single high-SNR MM basis function (cohort-mean) leads to more robust metabolite estimation (lower model residuals and AIC values) compared to MM strategies

with more degrees of freedom (Gaussian parametrization) or subject-specific MM information. Integration of multiple LCM analyses into a single statistical model potentially improves the robustness in the detection of underlying effects (e.g. metabolite vs age), reduces algorithm-based bias, and estimates algorithm-related variance.

## Introduction

Single-voxel proton MRS allows in-vivo research studies of brain metabolism[1,2]. At clinical field strength (≤3T), spectral modeling is hampered by poor spectral resolution as, particularly for short-echo-time (short-TE) spectra, metabolite signals overlap with a broad background consisting of fast-decaying macromolecule and lipid signals. Linear-combination modeling (LCM) is the consensus-recommended quantification method for short-TE spectra. LCM algorithms estimate spectra as a linear combination of metabolite and macromolecular (MM) basis function, maximizing use of prior knowledge to constrain the model solution[3].

Recent consensus on the modeling of short-TE spectra emphasizes that the MM basis functions included in the LCM must be either accurately parameterized by taking $T_1$ and $T_2$ evolution of the MMs into account, or directly measured with matching acquisition parameters [3,4]. However, acquiring MM spectra is time-consuming and technically challenging especially since stock sequences typically lack pre-inversion modules, and protocols for acquiring metabolite-nulled spectra are not widely available. This results in two common practices in the field, either: 1) MM spectra are measured in a small number of subjects and then averaged into a cohort-mean MM basis function to be included in the analysis of the whole cohort and subsequent studies[4] to minimize protocol duration; or 2) MM spectra are modeled using a default empirical parameterization as a series of Gaussians [5] as described in the most widely used LCM algorithm LCModel[6,7]. The latter approach is more commonly taken, as it does not require any additional time-consuming data acquisition or specialized processing, although it is not clear how adequate such parametrizations are.

Interestingly, it has not been investigated whether including subject-specific measured MMs (mMM) in the LCM has advantages over cohort-mean mMMs, possibly because prohibitively long acquisition times have disincentivized such a study, and current MRS analysis software does not provide easily accessible workflows to do so. A recent large-scale lifespan cohort[8,9] now provides sufficient publicly available data to compare the two strategies. This dataset further

allows investigation of other important issues of MM modeling in short-TE spectra to be investigated:

1. Parameterized vs. measured MM: Only a few low-n studies have systematically compared metabolite estimation between parameterized MM (pMM) and mMM modeling, or studied updated MM parameterizations[10–12].
2. Other studies focused on individual differences between measured MM spectra, but did not investigate the impact on the metabolite estimation[8,13].
3. LCM algorithms apply modeling parameters to the basis functions, including a single Gaussian linebroadening parameter to account for $B_0$ inhomogeneities in the MRS volume[6,14,15]. This practice becomes problematic when simulated metabolite basis functions are combined with a measured MM background, since the latter already has in-vivo linewidth. It might therefore be more appropriate to use two separate Gaussian linebroadening parameters (one for metabolites, one for MM).

The overarching goal of this study was to systematically investigate different strategies for the inclusion of MM signals for linear-combination modeling of short-TE PRESS spectra, most notably the use of single-subject MM data. We sought to substantiate expert-consensus recommendations on MM handling[3,4] and provide readily usable workflows for all strategies in our analysis pipeline 'Osprey'[14]. To this end, different MM modeling strategies were implemented and applied to a large lifespan dataset from healthy volunteers[8,9]. Macromolecular modeling strategies include cohort-mean and subject-specific measured macromolecules, the most commonly used Gaussian parametrizations, and the use of a single or two separate Gaussian linebroadening parameters. In the absence of a 'gold standard', the performance of each strategy was evaluated by comparing descriptive statistics of metabolite estimates, Akaike information criteria (AIC), model residuals, and variance partition analysis. Finally, we investigated whether the choice of MM model had an influence on the observation of metabolite-age associations.

# Methods

## Study participants & data acquisition

In this study, a cohort of 102 healthy volunteers was recruited with equal numbers of male and female participants in each decade of life—the 20s to 60s—following local IRB approval (Shandong Hospital, China, Provincial Hospital). Exclusion criteria included a history of neurological or psychiatric illness, and contraindications for MRI. Details of the acquisition protocol can be found in published studies of the same cohort[8,9]. Briefly, all participants were scanned on a Philips 3T MRI scanner (Ingenia CX, Philips Healthcare, The Netherlands) and the protocol included a $T_1$-weighted MP-RAGE scan with 1 $mm^3$ isotropic resolution for voxel positioning and tissue segmentation. Short-TE metabolite data were acquired using PRESS localization[16] (TR/TE 2000/30 ms, 30x26x26$mm^3$, 96 transients, 2048 datapoints, 2000 Hz sampling bandwidth, VAPOR water suppression[17]) in the posterior cingulate cortex (PCC). Subcutaneous lipid adjacent to the voxel was suppressed with a slice-selective saturation pulse (20 mm thickness). Additionally, metabolite-nulled MM data were acquired in the same voxel with an inversion time of 600 ms using an adiabatic hyperbolic-secant inversion pulse with a full-width half-maximum (FWHM) of 698 Hz applied at 1.9 ppm to minimize impact on the water signal, which was suppressed using Philips CHESS water suppression[18]. Water reference spectra were acquired for each participant without water suppression or pre-inversion.

## Data analysis

### *Pre-processing*

Data were analyzed in MATLAB (MATLAB R2022a, The MathWorks Inc., Natick, Massachusetts, United States) using Osprey (v.2.2.0), an end-to-end open-source MRS analysis toolbox. Pre-processing on the scanner included coil-combination, averaging, and eddy-current-correction using the water reference scan[19]. Water reference data were eddy-current-corrected in Osprey (since they are exported from the scanner without this correction). Residual water signal in the metabolite and metabolite-nulled spectra was removed with a Hankel singular decomposition (HSVD) filter[20]. As previously described[8], imperfectly-nulled metabolite signals in MM spectra were removed with a linear-combination modeling procedure using simulated metabolite signals (NAA, Cr, $CrCH_2$, Cho, Glu) and a highly flexible spline (0.1 ppm knot spacing) to model the

MM signals in the metabolite-nulled spectrum between 0.5 and 4.2 ppm. The fitted metabolite signals were subsequently subtracted from the spectra to yield 'clean' MM spectra. Finally, the clean MM spectra were modeled with a flexible spline model (again 0.1 ppm knot spacing) to generate a noise-free MM basis function for subsequent LCM of the metabolite spectra (**Supplementary Material 1**). Data quality metrics (SNR and linewidth of the NAA singlet) were calculated for the processed metabolite spectra. SNR was defined as the ratio of the NAA singlet peak height and the standard deviation of the frequency-domain spectrum between -2 and 0 ppm. LW was defined as the average of the simple FWHM and the FWHM of a Lorentzian peak model of the NAA singlet.

*Short-TE linear-combination modeling strategies*

Metabolite data were modeled using the Osprey LCM algorithm, using a basis set of 18 metabolite basis functions generated from a fully-localized 2D density-matrix simulation of a 101 x 101 spatial grid (field of view 50% larger than voxel) implemented in the cloud-based MATLAB toolbox 'MRSCloud'[21] derived from FID-A[22]. The following basis functions were included: ascorbate, aspartate, creatine, negative creatine methylene (-$CrCH_2$, to account for water suppression/relaxation), GABA, glycerophosphocholine (GPC), glutathione (GSH), Gln, Glu, mI, Lac, NAA, NAAG, phosphocholine, phosphocreatine, phosphoethanolamine (PE), Scyllo (sI), and taurine (**Figure 1**). Detailed descriptions of the frequency-domain LCM algorithm and parameter settings can be found elsewhere[5,14]. Briefly, metabolite spectra were analyzed between 0.5 and 4 ppm with a spline baseline knot spacing of 0.4 ppm. The model frequency range was different from the MM spectra to reduce possible confounds from the different water suppression techniques (CHESS for MM spectra; VAPOR for metabolite spectra)[8] and allow direct comparison to previous studies[5,23]. While the highly flexible (0.1 ppm knot spacing) spline model needs to fully capture the broad MM signals in the metabolite-nulled spectra, the 0.4-ppm knot spacing setting was chosen as the spline baseline is only required to account for low-frequency background fluctuations in the metabolite spectra. This setting for LCM of short-TE MRS in Osprey has previously led to good agreement with other LCM algorithms[5]. Model parameters of Osprey's frequency-domain LCM algorithm include amplitude estimates for the metabolite basis functions, frequency shifts, zero/first order phase correction, Gaussian and Lorentzian linebroadening, and cubic spline baseline coefficients. Water reference data were modeled with a

simulated water basis function and a 6-parameter model (amplitude, zero- and first-order phase, Gaussian and Lorentzian linebroadening, and frequency shift).

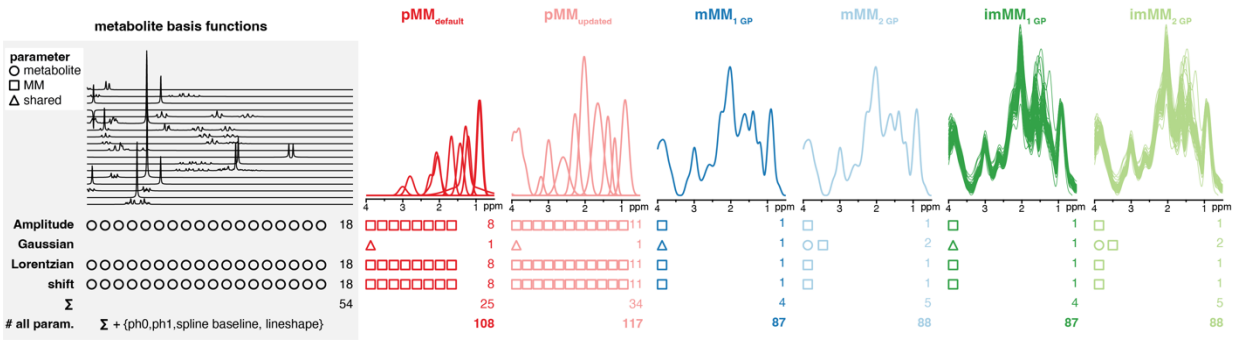


*Figure 1* – Strategies to include macromolecules in the LCM of short-TE MRS, including commonly used default ($pMM_{default}$ in bold red), updated Gaussian parameterization ($pMM_{updated}$ in light red) based on measured MM spectra, single measured MM based on the cohort mean ($mMM_{1\ GP}$ and $mMM_{2\ GP}$ in bold and light blue, respectively), and individual measured MM ($imMM_{1\ GP}$ and $imMM_{2\ GP}$ in bold and light green, respectively). Inclusion of a single Gaussian model parameter for metabolites is marked "1 GP" and models using separate parameters are marked "2 GP". The number of model parameters, and indicators whether those are shared between metabolite and MM basis *functions* (triangle) or separate (circle and square respectively for metabolite and MM) are shown below.

The centerpiece of this study is the comparison of different implementations to account for MMs in short-TE LCM (**Figure 1**). In general, each MM basis function has its own model parameters for the amplitude, frequency shift, Lorentzian linebroadening. The six strategies can be grouped into 'parameterized MM' (pMM) and 'measured MM' (mMM) strategies, and the mMM strategies have been implemented with one shared or two separate Gaussian linebroadening parameters for metabolites and MM:

- The default parametrization **$pMM_{default}$** model (**bold red**) contains 8 Gaussian basis functions to parameterize the MMs and lipids as previously described[5]. The parameterization is derived from the LCModel manual[7] without the definition of expectation values for the Lorentzian linebroadening and the frequency shift during the optimization and a simplified Lipid model at 1.3 ppm. Detailed amplitudes, frequency shifts, linewidth, and soft constraints for the LCM can be found in **Supplementary Material 2**. This parametrization is still the most widely used implementation and its performance has previously been described for a large multi-site dataset[5].

- The updated parametrization **$pMM_{updated}$** model (**light red**) incorporates a total of 11 MM basis functions which are generated by averaging the spline model of all metabolite-nulled spectra and modeling that as a linear combination of 14 Gaussian peaks - between 0.5 and 4.2 ppm - with the initial frequency shifts, as previously described[8]. This MM strategy does not include additional lipid peaks, as the averaged spline model did not allow for the separation of the broad peaks at 0.9 and 1.3 ppm. The Gaussian basis functions between 3.7 and 4.0 ppm overlapped substantially and were therefore summed to generate a single '$MM_{3.7\text{-}4.0}$' basis function, an approach described previously[24]. Again, detailed parametrization can be found in **Supplementary Material 2**.
- The cohort-mean measured **$mMM_{1\ GP}$** model (**dark blue**) has a single MM basis function generated by averaging the noise-free metabolite-nulled spectra from all participants. The same shared Gaussian lineshape parameter is applied to the metabolite and the MM basis function (therefore named $mMM_{1\ GP}$). This approach has the lowest number of model parameters and benefits from high signal-to-noise by using the averaged MM spectra. The creation of this across-age-cohort-mean MM basis function is only appropriate as no significant changes in the MM signals were observed as a function of age[8]. However, it enforces fixed ratios between the MM signals and is unable to capture any subject-specific variation of the MM signals. This approach has previously been employed in the same cohort[9] and closely corresponds to the MRS data analysis consensus recommendations[3,4].
- The cohort-mean measured **$mMM_{2\ GP}$** model (**light blue**) is identical $mMM_{1\ GP}$, except that two Gaussian lineshape parameters are included to separately model additional linewidth applied to metabolite basis functions and the MM basis function.
- The individual subject-specific measured **$imMM_{1\ GP}$** (**dark green**) uses the noise-free metabolite-nulled spectrum from each individual subject, instead of the cohort-averaged MM basis function. This strategy incorporates subject-specific MM variation.
- The subject-specific measured **$imMM_{2\ GP}$** model (**light green**) implements the same subject-specific MM basis function with separate Gaussian lineshape parameters applied to metabolite and MM basis functions.

All models are implemented in Osprey v2.2.0 and freely available on GitHub[25]. A summary page following the minimum reporting standards in MRS consensus paper[26] can be found in **Supplementary Material 3**.

## Quantification, visualization, and statistics

### *Quantification*

Water-referenced metabolite concentrations were calculated using tissue-specific water visibility and relaxation based on literature values[27,28] for each segmented tissue fraction of the voxel derived from the SPM12-based co-registration and segmentation of the $T_1$-weighted anatomical image and the MRS voxel[29].

### *Visualization*

The model performance and spectral characteristics arising from the systematic differences of each modeling strategy were visually assessed through the mean spectra, mean fit model, mean total MM (tMM) models, mean spline baseline, mean total background (tMM + spline baseline), and mean residuals (means taken across all datasets).

Metabolite estimates are visualized as raincloud plots[30] with median, 25$^{th}$ and 75$^{th}$ percentile ranges, individual estimates, smoothed distributions, mean and standard deviation to identify systematic differences between the modeling strategies. The corresponding coefficients of variation (CV) are reported as bar plots. Correlations between metabolite estimates derived using the different approaches were reported as bar plots representing Pearson's correlation coefficient, *r*. Statistical differences between all pairs of correlation coefficients were evaluated using a modified Fisher's Z procedure[31] as implemented in the cocor package[32] and corrected for multiple comparisons using Bonferroni correction. In addition, a correlation matrix comparing the correlation between the participant age and the metabolite/MM estimates for all different approaches was created. The correlation matrix includes Pearson's correlation coefficients, *r*. For significant associations after applying Bonferroni correction (treating each MM strategy as a separate analysis with a correction factor of 15), the directionality of the correlation is encoded as a color-coded ellipsoid, with higher associations represented by a narrower ellipsoid, i.e. a circle indicates there is no association (r = 0) and a line indicates perfect association (r = 1), additionally emphasized by the size of the ellipsoid (small ellipsoid ≡ small r). The p values were encoded by

the linewidth of the ellipsoid (the smaller the p value, the stronger the line). Metabolite-age associations were further tested for stability using a variable selection difference (VSD) approach by sampling random subsets of the data as implemented in the glmvsd package[33]. The VSD was calculated for all metabolites and MM strategies removing 5%, 20% and 50% of the subjects with 5000 simulations each. VSD scores close to 0 indicate that no additional predictor is needed as age is a stable predictor for the metabolite concentration even in randomly sampled subsets of the data. VSD scores closer to 1 indicate that age is a poor predictor for the metabolite concentration and additional predictors are needed. All plots and statistics were generated in R[34] (Version 4.1.3) in RStudio (Version 2022.02.01, Build 461, RStudio Inc.) using SpecVis[5], an open-source package to visualize linear-combination modeling results with the ggplot2 package[35]. All scripts and results are publicly available on the Open Science Framework[36].

*Statistics*

Differences in the mean and the variance of the metabolite level estimates were assessed between $pMM_{default}$ and all other MM strategies. The statistical tests were set up as paired without any further inference. Fligner-Killeen's test with a post-hoc pair-wise Bonferroni corrected Fligner-Killeen's test was employed to test differences in metabolite estimate variance. An ANOVA, or Welch's ANOVA (depending on whether variances were different or not) was employed to test differences in the means. Post-hoc analysis was performed with a Bonferroni corrected paired t-test using non-equal or equal variances, respectively.

*Variance partition analysis with linear mixed-effect model*

Linear mixed-effect (LME) models were set up as a repeated-measure analysis to determine variance partition coefficients to assess the contribution of MM strategy-, age-, sex- and participant-related contributions to the total variance of metabolite estimates as described previously[5,23,37,38]. Age and sex were defined as fixed effects while MM approach and participant were defined as random effects. The probability of observing the test statistic was evaluated against the null hypothesis, which was simulated by performing parametric bootstrapping (10,000 simulations)[39]. The resulting p-values were corrected for multiple comparison using the Benjamini-Yekutieli approach[40] which is less conservative than a Bonferroni correction, taking into account the dependency between the metabolite level estimates.

Model evaluation criteria

The performance of each modeling approach was evaluated using several metrics including the impact on the metabolite estimates, metabolite-age associations, as well as several quality metrics:

1. Visual inspection for characteristic spectral features included: Agreement between mean models, structured residual, flexibility and agreement of the spline baseline, tMM, and background (spline baseline + tMM).
2. Consistency of metabolite estimates: between-subject coefficients of variation (CV = SD/mean) for all metabolite estimates were calculated for each modeling approach. Between-subject CV was interpreted as a measure of modeling performance, assuming that increased CVs are mainly introduced by variability in the modeling and do not reflect biological meaningful variance of metabolite estimates.
3. Agreement in the metabolite estimation between the different modeling approaches were assessed via a correlation analysis.
4. Amplitude fit quality: The difference between the maximum and minimum of the residual was determined, and then normalized by the noise level[2]. This was done over the entire modeling range and termed relative residual.
5. AIC: The Akaike information criterion[41], which takes the number of model parameters into account, is defined as follows:

$$logLikelihood_i = -0.5 * (\log(2 * \pi) + 1 - \log(N_i) + \log(SSE_i/N_i))$$

$$AIC_i = -2 * logLikelihood_i + 2K_i$$

Here, $N_i$ is the number of points in the i[th] modeling strategy, $SSE_i$ is the sum of squared error (i.e., squared residual) of that strategy, and $K_i$ is the number of free model parameters for that strategy. No further corrections for amplitude soft-constraints were employed. Lower $AIC_i$ values indicate a more appropriate model. Subsequently, $\boldsymbol{\Delta AIC_i}$ scores were calculated as the difference of $AIC_i$ of modeling strategy *i* and the model with the lowest $AIC_{min}$:

$$\Delta AIC_i = AIC_i - AIC_{min}$$

6. Inter-class correlation coefficients (ICC) were calculated between the clean MM spectra and the tMM model from the metabolite spectra LCM, as well as the clean MM spectra and the sum of tMM and spline baseline (spbl) model for all subjects.
7. Age-metabolite and age-MM associations were assessed for all models to identify interactions between differences in the model attributing signal to metabolites, MM, or spline baseline, as well as possible bias in a specific approach.
8. LME models were used to determine variance partitions for MM strategy, age, sex, participant, and residual unexplained variance which allows to make inferences about all effects across all datasets and determine influential factors in the quantitative analysis of large-cohort data.

# Results

All 102 datasets were successfully analyzed. After visual inspection, one subject was removed due to a large visible ethanol signal and a second subject was removed due to unwanted out-of-volume echoes visible in the model residual leading to a final total of 100 datasets. The data quality assessment indicated consistently high spectral quality ($SNR_{NAA}$ = 151 ± 23; $LW_{NAA}$ = 6.7 ± 0.9 Hz) without lipid contamination.

Visualization of modeling

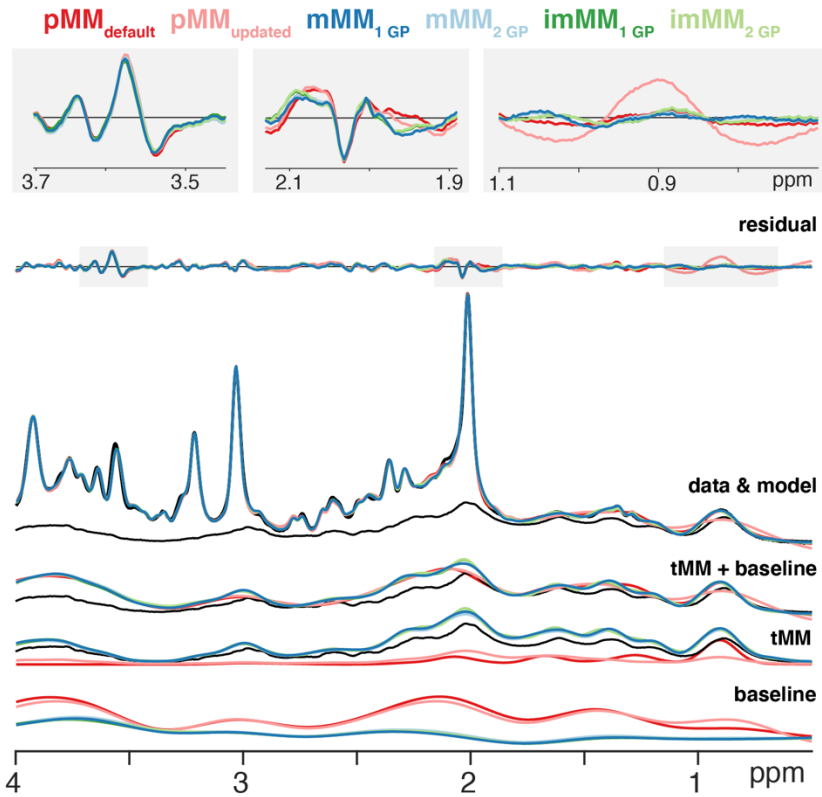


Figure 2 – Mean modeling results for all modeling strategies. Data and model agree well for all strategies; however, a substantial structured residual is apparent at 0.9 ppm for the $pMM_{updated}$ strategy. All six models are summarized with the mean results for residual, data (short-TE metabolite and MM), model, total MM model (tMM) + spline baseline model, tMM model, and spline baseline model. In addition, the mean of the 'clean' MM spectra is shown in black for reference. Three frequency regions with the largest residuals are magnified in the inlays at the top.

A summary of the data and modeling results is presented in **Figure 2**. Overall, a strong agreement between the mean of data and model is found for all modeling strategies. However,

there is a substantial structured signal in the mean residual at 0.9 ppm for the $pMM_{updated}$ strategy, indicating non-optimal parametrization of the $MM_{0.93}$ peak with a single MM basis function in this frequency region. The mean of the sum of the MM and baseline models agree well across all strategies, indicating that the combination of these two terms achieves comparable modeling of all broad non-metabolite signals, although the pMM strategies exhibit a broader and differently shaped signal in the 2-ppm region compared to the mMM strategies. Of note, there appears to be no systematic difference between the cohort-mean and the subject-specific mMM strategies, or between the strategies using 1 or 2 Gaussian linebroadening parameters. Upon closer inspection, it becomes strikingly obvious that the main differences appear between the pMM and mMM strategies, particularly with regard to how much signal they attribute to the baseline and the MM model, respectively, i.e. all pMM strategies attribute a lot more signal to the baseline model. In contrast, the mMM strategies exhibit a much flatter baseline model, and closely follow the shape of the mean mMM signal (except for a small scaling factor related to the different relaxation experienced by the MM between the metabolite-nulled and the metabolite spectra and the potential impact on the baseline introduced by the different water suppression schemes). Interestingly, the $pMM_{default}$ strategy agrees well with the mMM strategies at 0.9 ppm, but substantially less in the remaining frequency regions. The smaller residual could be related to a more accurate parametrization of the MM signal in this region, as two separate Gaussians ($MM_{0.91}$ & $Lip_{0.89}$) are included at 0.9 ppm for this strategy. The mean spline baseline models of the parameterized strategies have a higher number of more pronounced peaks (1.4, 2.2, 3.0, and 3.7 ppm) compared to the experimentally derived strategies indicating that the LCM algorithm estimates a larger portion of the overall signal as baseline for the former strategies.

Metabolite level estimates: Distribution and Correlation

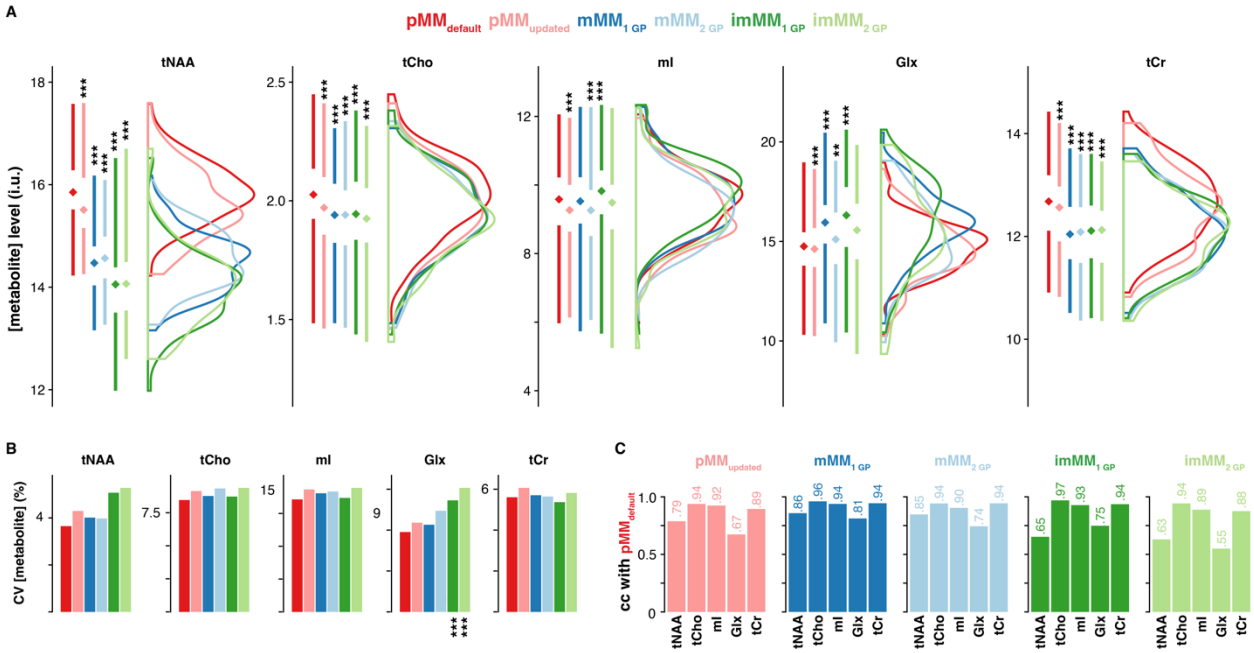


Figure 3 – Metabolite level estimates distribution and correlation between MM strategies for the major metabolites. (A) Metabolite estimate distributions major for all MM strategies. For the raincloud plots, box plots with median, interquartile range, and 25th/75th percentile, and smoothed distributions are shown. (B) Bar plots of the corresponding CV values. Asterisks indicate significant differences in the mean or variance between the $pMM_{default}$ and any other MM strategy (adjusted $p < 0.05$ = *, adjusted $p < 0.01$ = **, adjusted $p < 0.001$ = ***). (C) Pearson's correlation coefficient, r, for the correlation analysis between the $pMM_{default}$ and all other MM strategies. All correlations were found to be significant .

A summary analysis of the metabolite level estimates comparing the 'default parametrization' strategy $pMM_{default}$ to all other strategies is shown in **Figure 3** for the major metabolites and in **Figure 4** for all other metabolites. **Table 1** reports numerical summary of the results. Significant differences in mean metabolite level estimates between $pMM_{default}$ and any other strategy were found for almost all metabolites (**Figure 3A, 4A, and 4D**).

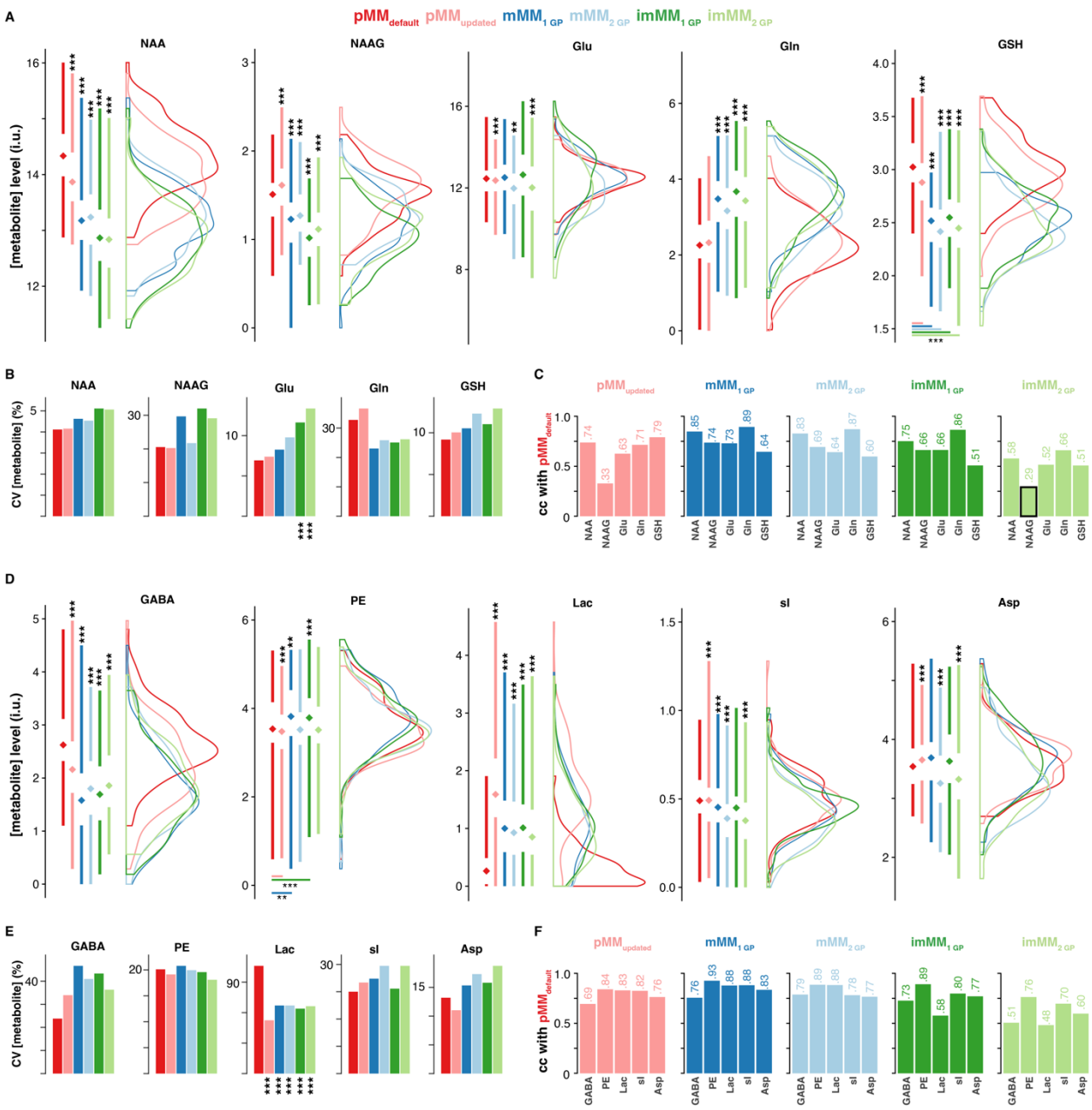


*Figure 4* – Metabolite level estimates distribution and correlation between MM strategies for all other metabolites. (A) Metabolite estimate distributions major for all MM strategies. For the raincloud plots, box plots with median, interquartile range, and 25th/75th percentile, and smoothed distributions are shown. (B) Bar plots of the corresponding CV values. Asterisks indicate significant differences in the mean or variance between the $pMM_{default}$ and any other MM strategy (adjusted $p < 0.05$ = *, adjusted $p < 0.01$ = **, adjusted $p < 0.001$ = ***). (C) Pearson's correlation coefficient, r, for the correlation analysis between the $pMM_{default}$ and all other MM strategies. All correlations were found to be significant .

Most notably, these include reductions in tNAA, tCr (**Figure 3A**), separate NAA and NAAG, and GSH (**Figure 4A**). A significant increase in the metabolite levels compared to the default parametrization strategy was found for Glx which is mainly driven by changes in the Gln estimates. No overall trend for the variance of the metabolite level estimates was observed. A significant increase in variance was found for three metabolites when using subject-specific measured MM spectra, namely Glx ($imMM_{1\ GP}$, $imMM_{2\ GP}$), Glu ($imMM_{1\ GP}$,$imMM_{2\ GP}$), and lactate ($pMM_{updated}$, $mMM_{1\ GP}$, $mMM_{2\ GP}$, $imMM_{1\ GP}$, $imMM_{2\ GP}$). This is potentially a result of the low SNR of individual MM spectra causing unwanted variance during the removal of residual metabolite signal during the MM clean-up. Lactate metabolite level estimates are substantially reduced for the $pMM_{default}$ strategy and exhibit significantly higher variance compared to all other MM strategies (**Figure 4D** and **E**).

In general, metabolite estimates correlated strongly ($r > 0.6$) for almost all metabolites between $pMM_{default}$ and all other strategies (**Figure 3C. 4C, and 4F**). The associations were particularly strong ($r > 0.85$) across all MM strategies for three (tCho, tCr, and mI) of the major metabolites either characterized by a strong singlet signal or total absence in the MM spectra. Lower associations ($r < 0.8$) were found for NAA, NAAG, and tNAA in $pMM_{updated}$, $imMM_{1\ GP}$ and $imMM_{2\ GP}$. Furthermore, Glx showed the weakest associations of the major metabolites between the MM strategies. Strategies generally agreed less well for low-concentration highly J-coupled metabolites (GSH, and NAAG) since their complex multiplet signals are harder to reliably separate from the broad background. Supporting this notion, weaker between -strategy correlation was also found for J-coupled metabolites whose residual contributions are difficult to reliably and accurately remove from the MM spectra (i.e. Glx. The analysis of the correlation coefficients (**Supplementary Material 4**) emphasizes these findings, indicating strong agreement for tCho, tCr, and mI. Significant differences where mainly found between $pMM_{default}$ and all other strategies, and between $imMM_{2\ GP}$ and all other strategies.

The introduction of separate Gaussian linewidth parameters for metabolites and MM resulted in significantly lower concentration estimates for 13 out of 30 metabolites, unchanged concentrations for 13 out of 30 metabolites and significantly higher concentrations for 4 out of 30 metabolites when compared to the MM strategies with a single shared Gaussian linewidth parameter and two separate Gaussian linewidth parameter . Metabolites with strong singlet signals were not affected by this, except for tNAA, driven primarily by changes in the NAAG

level estimation. Interestingly, the direction of change when introducing a second Gaussian parameter was similar for both the mMM and imMM strategies. 2-GP strategies did not result in changes in metabolite level variance compared to 1-GP strategies, except for the case of lactate where the additional Gaussian parameter reduced the observed variance of both cohort-mean and individual-measured models ($mMM_{1\ GP}$ vs $mMM_{2\ GP}$ and $imMM_{1\ GP}$ vs $imMM_{2\ GP}$).

Table 1 – Summary of the descriptive statistics of the metabolite level estimates. In each case, the upper number is the mean metabolite concentration, and the lower italic number is the standard deviation of the metabolite concentration across all subjects. Significant differences in mean or variance between a specific MM strategy and the $pMM_{default}$ strategy are marked in bold.

| metabolite | $pMM_{default}$ | $pMM_{updated}$ | $mMM_{1\ GP}$ | $mMM_{2\ GP}$ | $imMM_{1\ GP}$ | $imMM_{2\ GP}$ |
|---|---|---|---|---|---|---|
| tNAA | 15.89<br>*0.58* | **15.60**<br>*0.67* | **14.45**<br>*0.58* | **14.59**<br>*0.58* | **14.00**<br>*0.71* | **14.02**<br>*0.74* |
| tCho | 2.01<br>*0.17* | **1.97**<br>*0.18* | **1.94**<br>*0.17* | **1.93**<br>*0.18* | **1.95**<br>*0.17* | **1.92**<br>*0.18* |
| mI | 9.53<br>*0.98* | **9.29**<br>*1.04* | 9.59<br>*1.04* | **9.18**<br>*1.01* | **9.79**<br>*1.02* | 9.35<br>*1.06* |
| Glx | 14.66<br>*1.43* | **14.59**<br>*1.59* | **15.86**<br>*1.69* | **15.13**<br>*1.87* | **16.06**<br>***2.19*** | 15.37<br>***2.33*** |
| tCr | 12.66<br>*0.71* | **12.53**<br>*0.76* | **12.09**<br>*0.69* | **12.05**<br>*0.68* | **12.11**<br>*0.65* | **12.03**<br>*0.70* |
| NAA | 14.34<br>*0.59* | **13.95**<br>*0.58* | **13.19**<br>*0.61* | **13.23**<br>*0.60* | **12.91**<br>*0.66* | **12.84**<br>*0.65* |
| NAAG | 1.46<br>*0.30* | **1.58**<br>*0.32* | **1.18**<br>*0.35* | **1.29**<br>*0.28* | **1.00**<br>*0.32* | **1.10**<br>*0.32* |
| Glu | 12.42<br>*0.86* | **12.32**<br>*0.91* | 12.48<br>*1.03* | **11.96**<br>*1.17* | 12.55<br>***1.46*** | **11.97**<br>***1.60*** |
| Gln | 2.29<br>*0.75* | 2.32<br>*0.85* | **3.43**<br>*0.79* | **3.21**<br>*0.83* | **3.55**<br>*0.89* | **3.44**<br>*0.90* |
| GSH | 3.05<br>*0.28* | **2.89**<br>*0.29* | **2.47**<br>*0.26* | **2.44**<br>*0.30* | **2.54**<br>*0.28* | **2.48**<br>*0.32* |
| GABA | 2.69<br>*0.64* | **2.21**<br>*0.75* | **1.65**<br>*0.77* | **1.83**<br>*0.75* | **1.73**<br>*0.75* | **1.90**<br>*0.69* |
| PE | 3.63<br>*0.73* | **3.45**<br>*0.66* | **3.80**<br>*0.79* | 3.56<br>*0.71* | **3.78**<br>*0.74* | 3.59<br>*0.65* |
| Lac | 0.33 | **1.64** | **1.09** | **1.00** | **1.08** | **0.98** |

| | | | | | | |
|---|---|---|---|---|---|---|
| | *0.35* | ***0.86*** | ***0.73*** | ***0.67*** | ***0.69*** | ***0.65*** |
| sl | 0.50 | **0.48** | **0.46** | **0.38** | 0.45 | **0.38** |
| | *0.15* | *0.16* | *0.16* | *0.15* | *0.14* | *0.15* |
| Asp | 3.56 | **3.63** | 3.65 | **3.35** | 3.67 | **3.36** |
| | *0.47* | *0.40* | *0.56* | *0.58* | *0.58* | *0.63* |

Model evaluation criteria

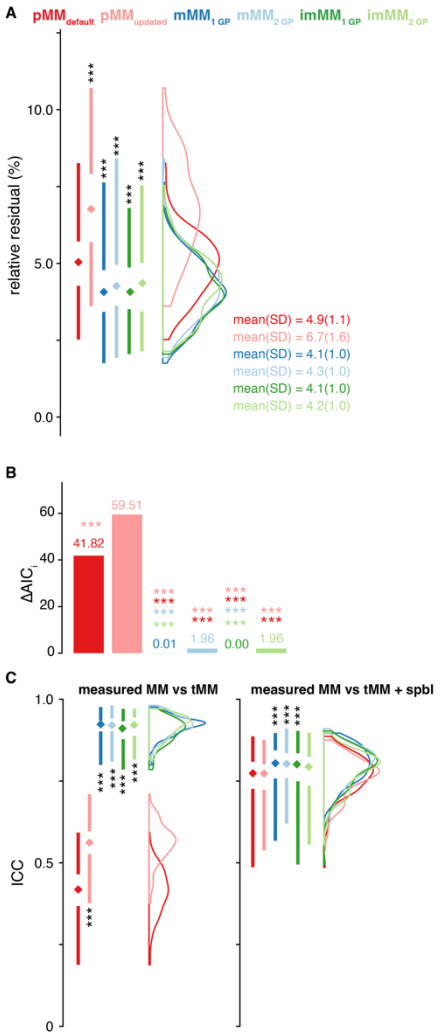


**Figure 5 –** Secondary analysis of residuals, and agreement between short-TE LCM total MM (tMM) model and individual MM spectra. Lower residual amplitudes and AIC scores were found for experimentally derived MM strategies. (A) Relative residual (%) for all MM strategies. (B) Mean ΔAIC values for all MM strategies. Asterisks indicate significant differences (adjusted $p < 0.001$ = ***) between a specific pair of MM strategies (color-coded). (C) ICC between the

individual's MM data and the short-TE LCM tMM or tMM + spbl model of the same individual. Asterisks indicate significant differences (adjusted $p < 0.05$ = *, adjusted $p < 0.001$ = ***).

The results of the model evaluation criteria in terms of model residual, AIC, and agreement between short-TE LCM tMM model and individual MM spectra are shown in **Figure 5**. A significant reduction of the model residual was found for all mMM strategies compared to the pMM strategies (**Figure 5A**). This suggests that an accurate representation (mMM and imMM) with fewer of degrees of freedom outperforms generalized representations (pMM) with a higher number of degrees of freedom. The $imMM_{1\ GP}$ strategy resulted in the overall lowest AIC, therefore, it was taken as the reference ($AIC_{min}$) for the ΔAIC calculation (**Figure 5B**). However, no significant difference in the AIC was found between the subject-specific $imMM_{1\ GP}$ and cohort-mean $mMM_{1\ GP}$ strategies, indicating comparable parsimony for both strategies. A significant but small increase in the ΔAIC value was found for the strategies with separate Gaussian linewidth parameters for metabolites and MM ($imMM_{2\ GP}$ & $mMM_{2\ GP}$) indicating that the possible advantage of one additional linewidth parameter was not justified by sufficiently high improvements of the model residual. Both parameterized strategies resulted in significantly higher ΔAIC values relative to the experimentally derived strategies due to the larger number of MM components and higher degree of freedom without offering lower model residuals than the mMM and imMM strategies.

The ICC analysis (**Figure 5C**) substantiates observations from Figure 2, i.e. poor agreement between the short-TE LCM tMM model estimated by the pMM strategies and the 'ground-truth' measured MM data. This indicates that the LCM performs relatively well in separating metabolite and broader background signals, however, it is unable to distinguish between spline baseline and MM signals, especially for the pMM strategies. When the sum of the MM and baseline models is considered, the agreement with the measured MM background improves, but remains significantly poorer for $pMM_{default}$ compared to 3 out of 4 measured MM strategies ($mMM_{1\ GP}$, $mMM_{2\ GP}$, $imMM_{1\ GP}$).

Finally, Gaussian lineshape parameter estimates did not differ between MM strategies. The mean shared Gaussian lineshape width were 8.94 ± 1.35 Hz for $pMM_{default}$, 8.93 ± 1.31 Hz for $pMM_{updated}$, 8.93 ± 1.37 Hz for $mMM_{1\ GP}$, and 8.93 ± 1.36 Hz for $imMM_{1\ GP}$. The mean separate Gaussian lineshape width for the metabolites were 8.91 ± 1.30 Hz for $mMM_{2\ GP}$ and 8.90 ± 1.34

for $imMM_{2\ GP}$. The mean separate Gaussian lineshape width for the MM were 5.09 ± 0.07 Hz for $mMM_{2\ GP}$ and 5.08 ± 0.08 Hz for $iMM_{2\ GP}$ and significantly smaller than for the metabolites. This supports the assumption that less Gaussian line broadening is needed for the experimentally derived MMs; however, this did not affect the metabolite Gaussian parameter.

Effect on metabolite-age associations

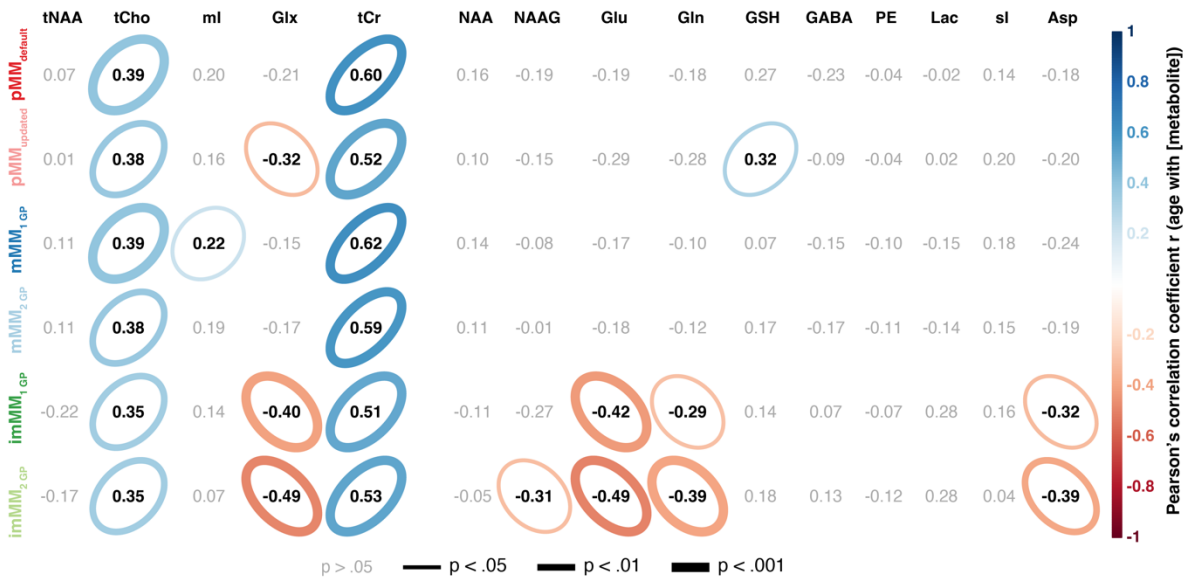


Figure 6 – Secondary analysis of metabolite-age associations for all MM strategies. Correlation matrix of Pearson's correlation coefficient, r, for the metabolite-age association. Results indicate stable metabolite-age associations for the major singlet metabolites, but more variable results for metabolites with stronger J-coupling. Significant correlations are indicated by color-coded ellipsoids with the directionality of r indicated by color and orientation and magnitude of r by the size of the ellipsoid. The p values were encoded by the linewidth of the ellipsoid (the smaller the p value the stronger the line). Bonferroni correction is employed for each MM strategy separately (correction factor of 15 metabolite level estimates).

The metabolite-age associations for all MM strategies are summarized in a correlation matrix in **Figure 6**. The two strong positive correlations between metabolite level and age for the two major singlet metabolites tCho (*r* between 0.35 and 0.39) and tCr (*r* between 0.51 and 0.62) are stable across all MM strategies with the strongest association found for the $mMM_{1\ GP}$ strategy. Metabolite-age associations are more variable between MM strategies for highly J-coupled metabolites that are affected by the characterization of the MM background for the frequency region > 3.2 ppm (see $MM_{3.7\text{-}4.0}$ age association in **Supplementary Material 5**). This is especially apparent for mI (*r* between 0.07 and 0.22), Glx (r between -0.15 and -0.49, affecting Glu and Gln

similarly), NAAG (*r* between -0.01 and -0.31), and GSH (*r* between 0.07 and 0.32). It is worth noting that changes in the tCr association may impact the interpretation, if creatine ratios are reported. Additionally, investigating changes in metabolites of interest in aging (such as GSH as a marker of oxidative stress[42,43]) may arrive at different conclusions depending on the MM modeling approach (although, note that quantification of GSH with short-TE LCM at 3T is controversial). Again, as found in **Figure 3B** and **4B**, the separability of metabolite signal and background is driving the differences in the metabolite-age associations, as for example mI appears to have lower variability as for example Glx and GSH. Similar to the changes for > 3.2 ppm frequency region, the variability in the non-significant correlation of age and tNAA may be explained by signal contributions in the 2 ppm frequency region being attributed to the MM or baseline (see $MM_{2.0}$ age association in **Supplementary Material 5**), especially as the $MM_{2.0}$ component is significantly associated with age for the pMM strategies.

The stability of the metabolite-age associations are summarized in **Supplementary Material 6.** VSD scores of 0 or close to 0 (Gln for $imMM_{1\ GP}$) were found in case of 5% and 20% data removal for all metabolite-age associations that were found to be significant (see Figure 6). Even upon removal of 50% of the data, the VSD remained within acceptable limits (0 for tCr, <0.06 for tCho, and <0.11 for all other) for those associations. The VSD of the remaining associations ranged between .11 and 0.91 indicating lower stability.

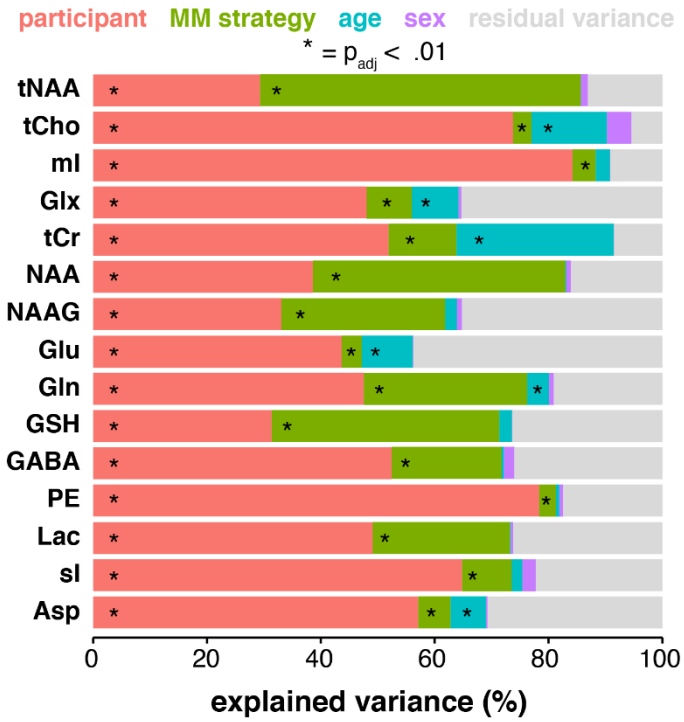


Figure 7 – Variance partition analysis for each metabolite across all MM strategies. The linear-mixed effect model includes fixed effects for age and sex, and random effects for participant and MM strategy. Significant effects are marked with an asterisk (adjusted $p < 0.01$ = *).

The variance partition analysis is summarized in **Figure 7** and **Table 2**. For most metabolites, the largest portion of the variance is explained by the participant level, representing biological variance between subjects. On average 'participant' explained 52.3% of variance, MM strategy 19.3%, age 5.2%, and sex 0.95% while 22.3% of variance was not accounted for by these factors. This indicates good responsive of all models to biological variance, significant differences in the metabolite estimates for different MM strategies contributing to overall variance, and no general age or sex 'pattern' across all metabolites. Choice of MM strategy explains a significant portion of the variance for all metabolites and is a stronger contributor to the overall variance than 'participant' for tNAA (56.3% vs 29.4%), NAA (44.4% vs 38.6%), and GSH (40% vs 31.4%). In addition, 43.7% of the variance of Glu is not explained by any of the included factors. Comparing this analysis, which combines all results in a single analysis, with the simpler correlation analysis separated by MM strategy (Figure 5) confirms some of the metabolite-age associations. For example, tCr and tCho show a strong impact of age, which was also consistently found across all MM strategies in the correlation analysis. In contrast to the correlation analysis, the

LME analysis also indicates significant contributions of age effects for Glx, Glu, Gln, and Asp which were found only for a subset of MM strategies in the correlation analysis. Further, no variance contribution from age was found for mI, NAAG, and GSH, which were in turn observed in the correlation analysis.

Table 2 - Variance partition estimation for each metabolite across all MM strategies. The linear-mixed effect model includes fixed effects for age, and sex and random effects for participant and MM strategy. Significant effects are marked with an asterisk (adjusted $p < 0.01$ indicated in bold).

| metabolite | participant | MM strategy | age | sex | residual |
|---|---|---|---|---|---|
| tNAA | **29.4** | **56.3** | 0 | 1.2 | 13.1 |
| tCho | **73.8** | **3.2** | **13.3** | 4.3 | 5.4 |
| mI | **84.3** | **4.0** | 2.5 | 0 | 9.2 |
| Glx | **48.1** | **8.0** | **8.2** | 0.5 | 35.3 |
| tCr | **51.9** | **11.9** | **27.6** | 0.1 | 8.5 |
| NAA | **38.6** | **44.4** | 0.2 | 0.8 | 16.1 |
| NAAG | **33.1** | **28.8** | 2.0 | 0.9 | 35.2 |
| Glu | **43.7** | **3.5** | **9.0** | 0.1 | 43.7 |
| Gln | **47.6** | **28.7** | **3.8** | 0.9 | 19 |
| GSH | **31.4** | **40.0** | 2.2 | 0.1 | 26.3 |
| GABA | **52.5** | **19.3** | 0.4 | 1.8 | 26 |
| PE | **78.4** | **2.9** | 0.6 | 0.7 | 17.4 |
| Lac | **49.1** | **24.1** | 0.1 | 0.4 | 26.2 |
| sI | **64.8** | **8.7** | 1.9 | 2.3 | 22.2 |
| Asp | **57.1** | **5.7** | **6.2** | 0.2 | 30.7 |
| **mean** | 52.3 | 19.3 | 5.2 | 0.95 | 22.3 |

# Discussion

We have presented a comparison of six different strategies to incorporate MM basis functions into short-TE LCM metabolite estimation applied to a large lifespan cohort. The major goals were: 1) to compare metabolite level estimates obtained with cohort-mean and subject-specific measured MM and different MM parametrizations; 2) to identify potential sources of differences between the strategies and how they affect metabolite-age associations. The key findings of our study are:

- Group-mean metabolite level estimates significantly differ between parameterized and experimentally derived MM strategies, most notably for tNAA, tCr and GSH. However, for most metabolites, the estimate variance did not change.
- Despite differences in the mean, metabolite estimates correlated strongly ($r > 0.6$) between the default MM parametrization strategy $pMM_{default}$ and all other MM strategies. Highly J-coupled metabolites showed weaker correlations between MM strategies than singlet signals.
- Experimentally derived MM strategies had better residuals and parsimony metrics than parameterized strategies, indicating greater agreement between data and model. This is especially intriguing since measured MM models have fewer model parameters and therefore fewer degrees of freedom. However, similar performance could possibly be achieved with more accurately parameterized MM basis functions.
- Metabolite-age associations were relatively stable across MM strategies for metabolites with major singlet signals, however, less so for highly J-coupled metabolites. Variance partition analysis indicated that up to 56.3% (tNAA) of metabolite level variance can be explained by the choice of MM strategy. This highlights the importance of choosing an appropriate MM modeling strategy on validity and interpretation of the results. The variance partition analysis further substantiated the metabolite-age associations for tCho, tCr, Glx, Glu, and Gln. Incorporating the choice of different modeling strategies into a global analysis may increase the robustness of its findings compared to a single correlation analysis.

In this study we took advantage of Osprey's modularity and its accessible LCM algorithm to create a workflow for directly incorporating subject-specific MM spectra and to introduce separate

Gaussian linebroadening parameters for metabolites and MM. These novel modifications highlight a key strength of open-source LCM workflows, since they would be much more challenging to do in closed-source or pre-compiled LCM algorithms. Our results did not demonstrate any substantial advantage conferred by the use of subject-specific MM data in terms of the stability of the age-metabolite association of tCr and tCho, but lead to substantial changes for tNAA, Glu, Gln, and Asp. However, it remains unclear whether this is an artifact introduced by remaining inaccuracies in the MM processing or whether this is an accurate estimation of true biological variability. This suggests that cohort-mean MM basis functions can be used in homogeneous populations and can be time-efficiently reused in similar populations instead of reacquiring for each study. For clinical populations with an underlying pathology affecting MM patterns, it is required to create a cohort-specific MM basis function for this population to achieve more accurate quantification – in addition to the MM basis function for the healthy controls. As a caveat, it is difficult to conclusively establish how many participants-worth of MM data are needed to generate a truly cohort-representative MM spectrum. In the case of highly heterogenous MM spectra within the clinical population, it may even be beneficial to use subject-specific MM. However, it remains unclear how many participants-worth of MM data would constitute a cohort-representative MM spectrum. An interesting strategy would be to acquire a short metabolite-nulled acquisition in every participant, with insufficient SNR to be individually interpretable, but sufficient when averaged across the cohort to generate an appropriate cohort-specific MM spectrum, instead of one long metabolite-nulled acquisition in only a few subjects. While metabolite estimates were significantly different, we did not find substantial differences in the age-metabolite associations when introducing an additional Gaussian linebroadening parameter for MM. Additionally, model residuals and ΔAIC did not improve, indicating no real advantage to this approach. The significant impact of the choice of MM modeling strategy on the short-TE LCM has been shown in several earlier studies[10–12]. Although these studies are either not performed at clinically relevant field strength (≤ 3T) or their statistical power is limited[10–12], we found evidence to support a number of their key findings. Confirming previous reports by Schaller et al.[10] using the LCModel algorithm[6], we found a significant increase in Glx estimates when using experimentally derived MM, however, in contrast to their results this effect was dominated by increased Gln estimates while Glu remained unaffected. We further substantiated their findings that NAA and tNAA estimates decrease when using measured MMs or an updated MM parametrization.

This is mostly related to the differences in the amplitude of the $MM_{2.0}$ peak which is notably smaller in the $pMM_{default}$ models than in all measured MM spectra. However, it remains unclear whether the large 2-ppm signals in the mMM data represent 'real' MM contributions, or are an artifact or unaddressed metabolite signal from the clean-up process. A recently presented method using strongly diffusion-weighted MRS to determine the MM background yielded much smaller $MM_{2.0}$ signals, more distinct MM peaks in the 3.5 to 4 ppm region, and narrower lines in general[44] compared to the IR method used in our study or previously used saturation-recovery methods[13]. Another potential approach using IR is to acquire a TI-series or 2D-J-spectra at multiple fixed TI in combination with multidimensional modeling that allows separation of metabolite and MM concentration and relaxation parameters. However, multi-dimensional data are more challenging to model[45]. It is unclear which of the approaches is more appropriate and less error-prone to estimate the MM background. Another similar study on the impact of the MM approach in short-TE LCM by Gottschalk et al.[11] reported comparable changes in metabolite estimates using the QUEST LCM algorithm[46] with similar directionality of change, e.g. increase in GSH estimates, when comparing modeling approaches with experimentally-derived MM strategies and the QUEST subtraction approach. Confirming findings from that study, we found evidence for a substantial advantage of the experimentally-derived MM strategies over parameterized approaches for the quantification of lactate, which is typically a very small signal on the shoulder of a broad MM peak around 1.3 ppm[11]. Both studies conclude that effects they observe are unlikely to affect the outcome in MRS application studies, however, there is no analysis directly proving this assumption. Both studies featured comparably small samples (11 for Schaller et al., and 20 for Gottschalk et al.) from a narrow age range, which is a substantial limitation to the generalizability of their findings to clinical and age-related studies. In contrast, we studied the impact of the MM strategy choice in a large cohort across the lifespan and unequivocally showed a major influence on the observed metabolite-age associations, especially for highly J-coupled metabolites with strong relevance in aging (e.g. GSH).

A third study by Hofmann et al.[13] used a saturation-recovery-based method to measure metabolite and MM spectra simultaneously including 40 healthy subjects with three age groups (< 25, 25-55, >55 years), but did not report metabolite quantification results.

In comparison to the most widely used LCM algorithm LCModel, Osprey's algorithm uses an unregularized spline baseline model, no prior distributions for the Lorentzian lineshape parameters, and single Gaussian MM basis functions for the parameterized approach. The advantages of using a single MM basis function may be more pronounced for this less constrained implementation as it strongly reduces the parameter space for the LCM algorithm. This additionally explains the relatively poor performance of the $pMM_{updated}$ strategy, e.g., for the $MM_{0.91}$ peak as the updated strategy only includes a single basis function around 0.9 ppm as opposed to two for the $pMM_{default}$ strategy ($MM_{0.92}$ & $Lip_{0.9}$). Additionally, the original LCModel algorithm includes range of frequencies and FWHM for the Gaussian peaks, as well as expectation values for the Lorentzian lineshape parameters which introduce more freedom to the algorithm to model those signals compared to Osprey. It would be interesting, but beyond the scope of this study, to compare different LCM algorithms, as previously[5] but with the measured MM spectra. It is possible that the introduction of a regularized baseline such as in LCModel or more advanced baseline approaches as in ABFit[47] or elsewhere[12] could improve the performance of parameterized MM estimation during short-TE LCM and allow for separation of metabolite, MM, and baseline signals. Apart from regularization terms the flexibility of a spline baseline can also be controlled by the density of the spline knot spacing and has been shown to have major impact on the quantification[48,49]. This is especially the case if separate Gaussian MM basis functions are used. In this study we used Osprey's default spbl knotspacing of 0.4 ppm which resulted in moderate baseline flexibility for the experimentally derived MM strategies and a good agreement in the combined [total MM + spline baseline] model for all strategies. However, increasing the spbl knotspacing could potentially further improve the performance of the experimentally derived MM strategies as the underlying MM signals are sufficiently described by the single MM basis function.

MM spectra have much broader, smaller, and less well-defined signals than metabolite spectra, and they inevitably still contain contributions from metabolites that are not perfectly nulled, particularly in a single-inversion recovery experiment because of differences in $T_1$ relaxation. Therefore, processing, removal of residual metabolite signals (clean-up), and quantification are crucial, but may suffer from imperfections. Potential issues are accurate frequency referencing due to the broader signals, residual metabolite signals due to imperfect metabolite-nulling[10,11] and their insufficient removal during post-processing, or an insufficient number of splines to

generate the noise-free clean MM spectra. While there were no obvious residual metabolite signals in the MM spline model, the higher variance of tNAA and Glx estimates for the subject-specific mMM strategies suggests greater variability of residual metabolite signals or imperfect clean-up of the single-subject MM spectra. $T_1$ differences between moieties may be implicated, and the use of moiety-specific basis functions during clean-up might reduce residual metabolite signals. Double-inversion recovery approaches might improve the consistency of metabolite nulling, however, at the cost of greater $T_1$-weighting of the MM signals. To reduce $T_1$-weighting effects diffusion-weighted metabolite-nulling could be used which is less susceptible to $T_1$ differences between metabolites or introduced by aging[44,50]. Additionally, the MM derived with metabolite nulling will differ from the MM background in the metabolite spectra by a $T_1$ relaxation factor. This is accounted for during LCM with a single linear amplitude scaling parameter for the MM basis function. While this is consensus-recommended best practice, it obviously requires the assumption that all MM signals relax with the same $T_1$, which may not be justified. Finally, another interesting approach to account for MM signals is to generate MM-nulled spectra with multiple-IR methods[51]. While this approach reduces the overall SNR of the spectra it significantly reduces the contributions of MMs, does not require separate acquisition of MM data, and could therefore improve the quantification of the remaining metabolite signals.

## Perspective for extension of multi-LCM approaches

This study is, to the best of the authors' knowledge, the first study to explicitly consider the additional variance introduced from different LCM strategies and settings in the final statistical analysis to model biological effects in the cohort, in this case metabolite-age associations. This 'meta-LCM' approach could prove to be more robust to model-based bias than a statistical analysis based on a single model, as seen in the differences observed in the separate correlation matrix. A novel generalized LCM analysis fully capturing model-related variance should aggregate a large number of diverse modeling strategies, in contrast to the few drastically different approaches presented here, which resulted in a large portion of the overall variance being attributed to the MM strategy for several metabolites. These diverse strategies may include different signal parametrizations (arbitrary lineshape as in Osprey[14] and LCModel[6], asymmetric lineshape as in ABFit[47], number of lineshape parameters), MM approaches (Gaussian basis functions, Voigt basis functions, mean/individually measured MM spectra), background signal descriptions (spline

functions as in Osprey[14] and LCModel[6], polynomials like in FSL-MRS, subtraction techniques as in QUEST[15,52] and Tarquin), parameter regularization, and model domain (time vs frequency domain, combined time and frequency domain, real- or complex-valued data). With ever increasing computational resources, a 'multi-model' meta analysis could lead to more robust metabolite estimation and provide a better estimate of estimation uncertainties related to the choice of modeling strategy.

## Limitations

A major limitation of the study, and in-vivo MRS in general, is the absence of a 'ground truth' of metabolite level estimates to validate LCM results against. As in our previous studies[5,53], we evaluated the performance of the different modeling strategies from a combination of estimate variance, fit residuals, parsimony scores, and robustness of observed metabolite-age associations. However, low variance or AICs do not reflect higher accuracy and may rather indicate insufficient responsiveness to real biological variance. The use of simulated spectra as a ground truth is promising as a validation strategy[54], but can only succeed if synthetic data are truly representative of in-vivo conditions. Another limitation is the single LCM algorithm Osprey that we used here, which, while conceptually and in performance[5] similar to LCModel, does not feature regularization terms on the baseline or the lineshape, and features fewer metabolite soft constraints. The data in this study are of exceptionally high spectral quality (high SNR, narrow linewidth, and no lipid contamination) and our observations and conclusions may substantially differ for spectra of lower spectral quality (low SNR, broader linewidth, and lipid contamination). Systematic differences in the baseline due different water suppression schemes could affect the model performance. However, such differences are accounted for by the spline baseline and could explain differences in the background signals of the metabolite and the metabolite-nulled spectra. Finally, since this study focuses on MM modeling strategies, we did not include a detailed interpretation and discussion of associations between metabolite levels, age and sex, which can be found elsewhere[9].

## Conclusion

Inclusion of a single high-SNR MM basis function derived from the cohort-mean of measured metabolite-nulled spectra lead to more robust metabolite estimation than Gaussian parametrizations with more degrees of freedom. Further, it can be included in future studies of healthy subjects making it more time-efficient than single-subject acquisition with minimal impact on metabolite quantification. While there were systematic differences of certain metabolite estimates (tNAA, Glx) between MM strategies, metabolite-age associations (particularly tCho, tCr) were relatively stable. Agreement between MM strategies was generally stronger for singlet signals than for J-coupled signals.

# References


1. Öz G, Alger JR, Barker PB, et al. Clinical Proton MR Spectroscopy in Central Nervous System Disorders. *Radiology*. 2014;270(3):658-679. doi:10.1148/radiol.13130531

2. Wilson M, Andronesi O, Barker PB, et al. *Methodological Consensus on Clinical Proton MRS of the Brain: Review and Recommendations*. Vol 82. John Wiley and Sons Inc.; 2019. doi:10.1002/mrm.27742

3. Near J, Harris AD, Juchem C, et al. Preprocessing, analysis and quantification in single-voxel magnetic resonance spectroscopy: experts' consensus recommendations. *NMR Biomed*. 2020;34:e4257. doi:10.1002/nbm.4257

4. Cudalbu C, Behar KL, Bhattacharyya PK, et al. Contribution of macromolecules to brain 1H MR spectra: Experts' consensus recommendations. *NMR Biomed*. 2021;34(5):e4393. doi:10.1002/nbm.4393

5. Zöllner HJ, Považan M, Hui SCN, Tapper S, Edden RAE, Oeltzschner G. Comparison of different linear-combination modeling algorithms for short-TE proton spectra. *NMR Biomed*. 2021;34(4):e4482. doi:https://doi.org/10.1002/nbm.4482

6. Provencher SW. Estimation of metabolite concentrations from localized in vivo proton NMR spectra. *Magn Reson Med*. 1993;30(6):672-679. doi:10.1002/mrm.1910300604

7. Provencher S. LCModel & LCMgui User's Manual. LCModel & LCMgui User's Manual. http://s-provencher.com/pub/LCModel/manual/manual.pdf. Published 2020. Accessed April 28, 2020.

8. Hui SCN, Gong T, Zöllner HJ, et al. The macromolecular MR spectrum does not change with healthy aging. *Magn Reson Med*. 2022;87(4):1711-1719. doi:10.1002/mrm.29093

9. Gong T, Hui SCN, Zöllner HJ, et al. Neurometabolic timecourse of healthy aging. *bioRxiv*. June 2022. doi:10.1101/2022.06.08.495050

10. Schaller B, Xin L, Cudalbu C, Gruetter R. Quantification of the neurochemical profile using simulated macromolecule resonances at 3 T. *NMR Biomed*. 2013;26(5):593-599. doi:10.1002/nbm.2896

11. Gottschalk M, Lamalle L, Segebarth C. Short-TE Iocalised 1H MRS of the human brain at 3T: Quantification of the metabolite signals using two approaches to account for macromolecular signal contributions. *NMR Biomed*. 2008;21(5):507-517. doi:10.1002/nbm.1219

12. Zhang Y, Shen J. Smoothness of in vivo spectral baseline determined by mean-square error. *Magn Reson Med*. 2014;72(4):913-922. doi:10.1002/mrm.25013

13. Hofmann L, Slotboom J, Boesch C, Kreis R. Characterization of the macromolecule baseline in localized 1H-MR spectra of human brain. *Magn Reson Med*. 2001;46(5):855-863. doi:10.1002/mrm.1269

14. Oeltzschner G, Zöllner HJ, Hui SCN, et al. Osprey: Open-source processing, reconstruction & estimation of magnetic resonance spectroscopy data. *J Neurosci Methods*. 2020;343:108827. doi:10.1016/j.jneumeth.2020.108827

15. Wilson M, Reynolds G, Kauppinen RA, Arvanitis TN, Peet AC. A constrained least-squares approach to the automated quantitation of in vivo 1H magnetic resonance spectroscopy data. *Magn Reson Med*. 2011;65(1):1-12.

16. Bottomley P. *Selective Volume Method for Performing Localized NMR Spectroscopy*. Vol 3.; 1985. doi:10.1016/0730-725X(85)90032-3

17. Tkáč I, Starčuk Z, Choi IY, Gruetter R. In vivo 1H NMR spectroscopy of rat brain at 1 ms echo time. *Magn Reson Med*. 1999;41(4):649-656. doi:10.1002/(SICI)1522-2594(199904)41:4<649::AID-MRM2>3.0.CO;2-G

18. Haase A, Frahm J, Hanicke W, Matthaei D. 1H NMR chemical shift selective (CHESS) imaging. *Phys Med Biol*. 1985;30(4):341-344. doi:10.1088/0031-9155/30/4/008

19. Klose U. In vivo proton spectroscopy in presence of eddy currents. *Magn Reson Med*. 1990;14(1):26-30. doi:10.1002/mrm.1910140104

20. Barkhuijsen H, de Beer R, van Ormondt D. Improved algorithm for noniterative time-domain model fitting to exponentially damped magnetic resonance signals. *J Magn Reson 1969*. 1987;73(3):553-557. doi:10.1016/0022-2364(87)90023-0

21. Hui SCN, Saleh MG, Zöllner HJ, et al. MRSCloud: a Cloud-based MR Spectroscopy Tool for Basis Set Simulation. March 2022:2022.03.22.485310. doi:10.1101/2022.03.22.485310

22. Simpson R, Devenyi GA, Jezzard P, Hennessy TJ, Near J. Advanced processing and simulation of MRS data using the FID appliance (FID-A)—An open source, MATLAB-based toolkit. *Magn Reson Med*. 2015;77(1):23-33. doi:10.1002/mrm.26091

23. Považan M, Mikkelsen M, Berrington A, et al. Comparison of Multivendor Single-Voxel MR Spectroscopy Data Acquired in Healthy Brain at 26 Sites. *Radiology*. 2020;295(1):191037. doi:10.1148/radiol.2020191037

24. Považan M, Strasser B, Hangel G, et al. Simultaneous mapping of metabolites and individual macromolecular components via ultra-short acquisition delay 1H MRSI in the brain at 7T. *Magn Reson Med*. 2018;79(3):1231-1240. doi:10.1002/mrm.26778

25. Osprey GitHub repository. Osprey GitHub repository. https://github.com/schorschinho/osprey. Published 2020. Accessed May 27, 2020.

26. Lin A, Andronesi O, Bogner W, et al. Minimum Reporting Standards for in vivo Magnetic Resonance Spectroscopy (MRSinMRS): Experts' consensus recommendations. *NMR Biomed*. 2021;34(5):e4484. doi:10.1002/nbm.4484

27. Gasparovic C, Song T, Devier D, et al. Use of tissue water as a concentration reference for proton spectroscopic imaging. *Magn Reson Med*. 2006;55(6):1219-1226. doi:10.1002/mrm.20901

28. Wansapura JP, Holland SK, Dunn RS, Ball WS. NMR relaxation times in the human brain at 3.0 Tesla. *J Magn Reson Imaging*. 1999;9(4):531-538. doi:10.1002/(SICI)1522-2586(199904)9:4<531::AID-JMRI4>3.0.CO;2-L

29. Friston K. *Statistical Parametric Mapping: The Analysis of Functional Brain Images*. Academic Press; 2007. http://books.google.com/books?id=KZZcLqkxhFIC%5Cnpapers://8fdc0079-0571-40b9-b7fa-84608563a121/Paper/p10618.

30. Allen M, Poggiali D, Whitaker K, Marshall TR, Kievit RA. Raincloud plots: a multi-platform tool for robust data visualization. *Wellcome Open Res*. 2019;4:63. doi:10.12688/wellcomeopenres.15191.1

31. Hittner JB, May K, Silver NC. A Monte Carlo evaluation of tests for comparing dependent correlations. *J Gen Psychol*. 2003;130(2):149-168. doi:10.1080/00221300309601282

32. Diedenhofen B, Musch J. cocor: A Comprehensive Solution for the Statistical Comparison of Correlations. *PLOS ONE*. 2015;10(4):e0121945. doi:10.1371/journal.pone.0121945

33. Nan Y, Yang Y. Variable Selection Diagnostics Measures for High-Dimensional Regression. *J Comput Graph Stat*. 2014;23(3):636-656. doi:10.1080/10618600.2013.829780

34. R Core Team. *R: A Language and Environment for Statistical Computing*. Vienna, Austria: R Foundation for Statistical Computing; 2017. https://www.R-project.org/.

35. Wickham H. *Ggplot2: Elegant Graphics for Data Analysis*. Springer-Verlag New York; 2009. http://ggplot2.org.

36. Zöllner HJ. Cohort-mean measured macromolecules lead to more robust linear-combination modeling than subject-specific or parameterized ones. June 2022. doi:10.17605/OSF.IO/7DXNM

37. Mikkelsen M, Barker PB, Bhattacharyya PK, et al. Big GABA: Edited MR spectroscopy at 24 research sites. *NeuroImage*. 2017;159:32-45. doi:10.1016/j.neuroimage.2017.07.021

38. Mikkelsen M, Rimbault DL, Barker PB, et al. Big GABA II: Water-referenced edited MR spectroscopy at 25 research sites. *NeuroImage*. 2019;191:537-548. doi:10.1016/J.NEUROIMAGE.2019.02.059

39. Halekoh U, Højsgaard S. A Kenward-Roger Approximation and Parametric Bootstrap Methods for Tests in Linear Mixed Models The R Package pbkrtest. *J Stat Softw*. 2014;59(1):1-32. doi:10.18637/jss.v059.i09

40. Benjamini Y, Yekutieli D. The control of the false discovery rate in multiple testing under dependency. *Ann Stat*. 2001;29(4):1165-1188. doi:10.1214/aos/1013699998

41. Akaike H. A new look at the statistical model identification. *IEEE Trans Autom Control*. 1974;19(6):716-723. doi:10.1109/TAC.1974.1100705

42. Hupfeld KE, Hyatt HW, Alvarez Jerez P, et al. In Vivo Brain Glutathione is Higher in Older Age and Correlates with Mobility. *Cereb Cortex*. 2021;31(10):4576-4594. doi:10.1093/cercor/bhab107

43. Bottino F, Lucignani M, Napolitano A, et al. In Vivo Brain GSH: MRS Methods and Clinical Applications. *Antioxidants*. 2021;10(9):1407. doi:10.3390/antiox10091407

44. Şimşek K, Döring A, Pampel A, Möller HE, Kreis R. Macromolecular background signal and non-Gaussian metabolite diffusion determined in human brain using ultra-high diffusion weighting. *Magn Reson Med*. July 2022:1-16. doi:10.1002/mrm.29367

45. Hoefemann M, Bolliger CS, Chong DGQ, van der Veen JW, Kreis R. Parameterization of metabolite and macromolecule contributions in interrelated MR spectra of human brain using multidimensional modeling. *NMR Biomed*. 2020;33(9):e4328. doi:10.1002/nbm.4328

46. Graveron-Demilly D. Quantification in magnetic resonance spectroscopy based on semi-parametric approaches. *Magn Reson Mater Phys Biol Med*. 2014;27(2):113-130. doi:10.1007/s10334-013-0393-4

47. Wilson M. Adaptive Baseline Fitting for 1H MR Spectroscopy Analysis. *bioRxiv*. February 2020:2020.02.17.949495. doi:10.1101/2020.02.17.949495

48. Giapitzakis IA, Borbath T, Murali-Manohar S, Avdievich N, Henning A. Investigation of the influence of macromolecules and spline baseline in the fitting model of human brain spectra at 9.4T. *Magn Reson Med*. 2019;81(2):746-758. doi:10.1002/mrm.27467

49. Marjańska M, Terpstra M. Influence of fitting approaches in LCModel on MRS quantification focusing on age-specific macromolecules and the spline baseline. *NMR Biomed*. November 2019:e4197. doi:10.1002/nbm.4197

50. Kunz N, Cudalbu C, Mlynarik V, Hüppi PS, Sizonenko SV, Gruetter R. Diffusion-weighted spectroscopy: A novel approach to determine macromolecule resonances in short-echo time 1H-MRS. *Magn Reson Med*. 2010;64(4):939-946. doi:10.1002/mrm.22490

51. Knight-Scott J. Application of Multiple Inversion Recovery for Suppression of Macromolecule Resonances in Short Echo Time 1H NMR Spectroscopy of Human Brain. *J Magn Reson*. 1999;140(1):228-234. doi:10.1006/jmre.1999.1799

52. Poullet JB, Sima DM, Simonetti AW, et al. An automated quantitation of short echo time MRS spectra in an open source software environment: AQSES. *NMR Biomed*. 2007;20(5):493-504. doi:10.1002/nbm.1112

53. Zöllner HJ, Tapper S, Hui SCN, Barker PB, Edden RAE, Oeltzschner G. Comparison of linear combination modeling strategies for edited magnetic resonance spectroscopy at 3 T. *NMR Biomed*. 2021:e4618. doi:10.1002/nbm.4618

54. Marjańska M, Deelchand DK, Kreis R, Team the 2016 IMSGFC. Results and interpretation of a fitting challenge for MR spectroscopy set up by the MRS study group of ISMRM. *Magn Reson Med*. 2022;87(1):11-32. doi:10.1002/mrm.28942

## Declaration of competing interests

The authors have nothing to declare.

## Acknowledgement

This work is supported by NIH grants R00 AG062230, P41 EB031771 R01 EB016089, R01 EB023963, R21A G060245, and R21 EB033516.

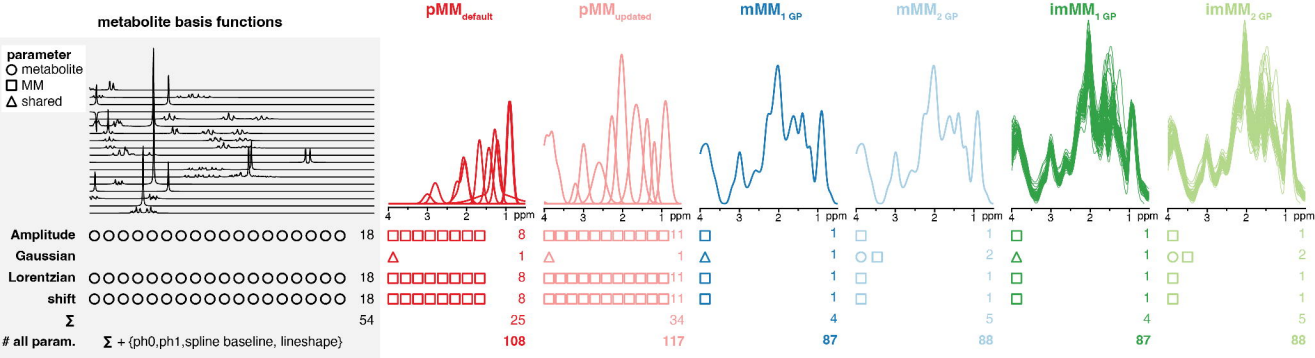
metabolite basis functions
parameter
metabolite
MM
shared
pMM default
pMM updated
mMM 1 GP
mMM 2 GP
imMM 1 GP
imMM 2 GP
4 3 2 1 ppm
Amplitude 18 8 11 1 1 1 1
Gaussian 1 1 1 2 1 2
Lorentzian 18 8 11 1 1 1 1
shift 18 8 11 1 1 1 1
Σ 54 25 34 4 5 4 5
# all param. Σ + {ph0,ph1,spline baseline, lineshape} 108 117 87 88 87 88

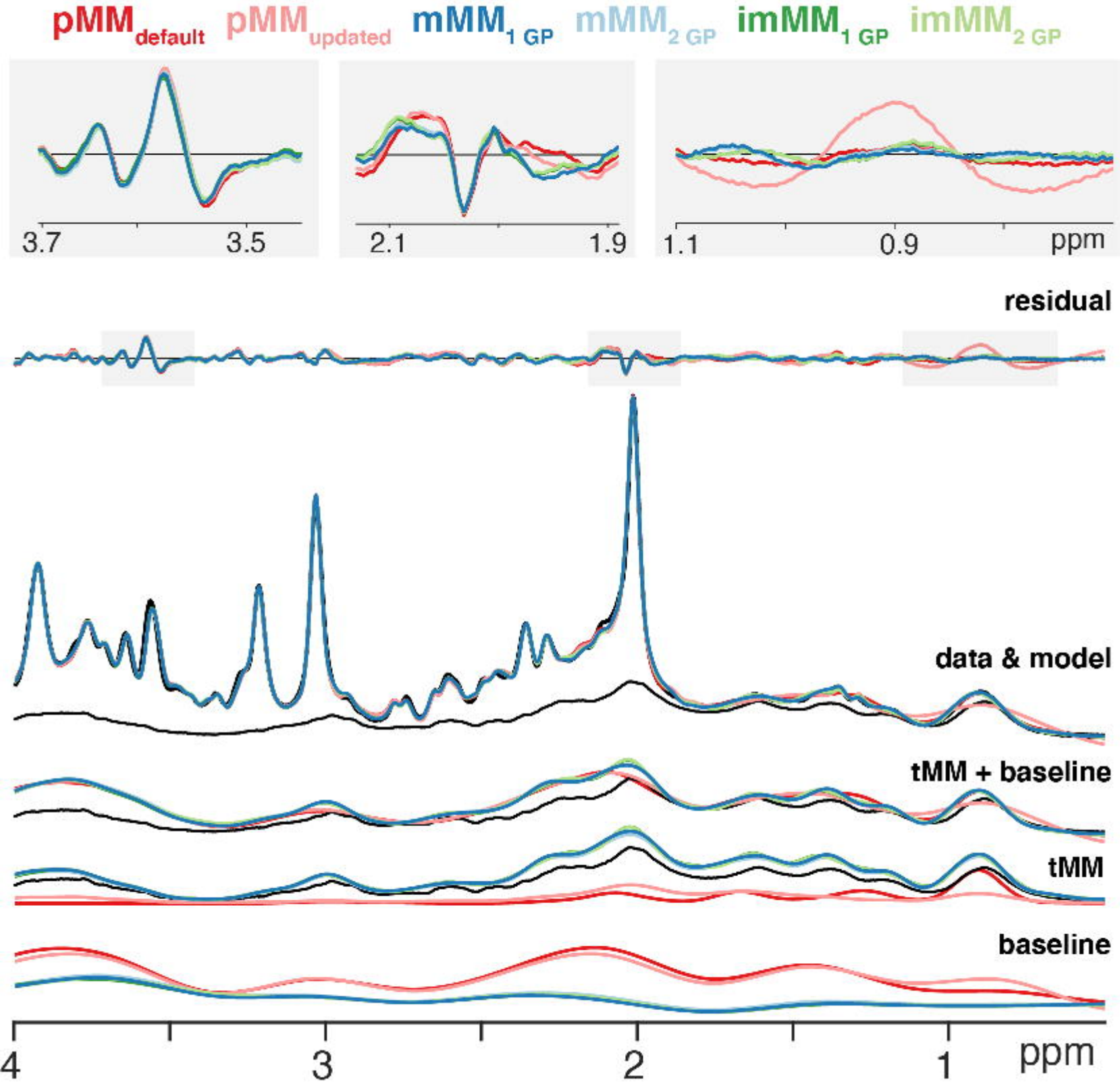
pMM default
pMM updated
mMM 1 GP
mMM 2 GP
imMM 1 GP
imMM 2 GP
3.7
3.5
2.1
1.9
1.1
0.9
ppm
residual
data & model
tMM + baseline
tMM
baseline
4
3
2
1
ppm

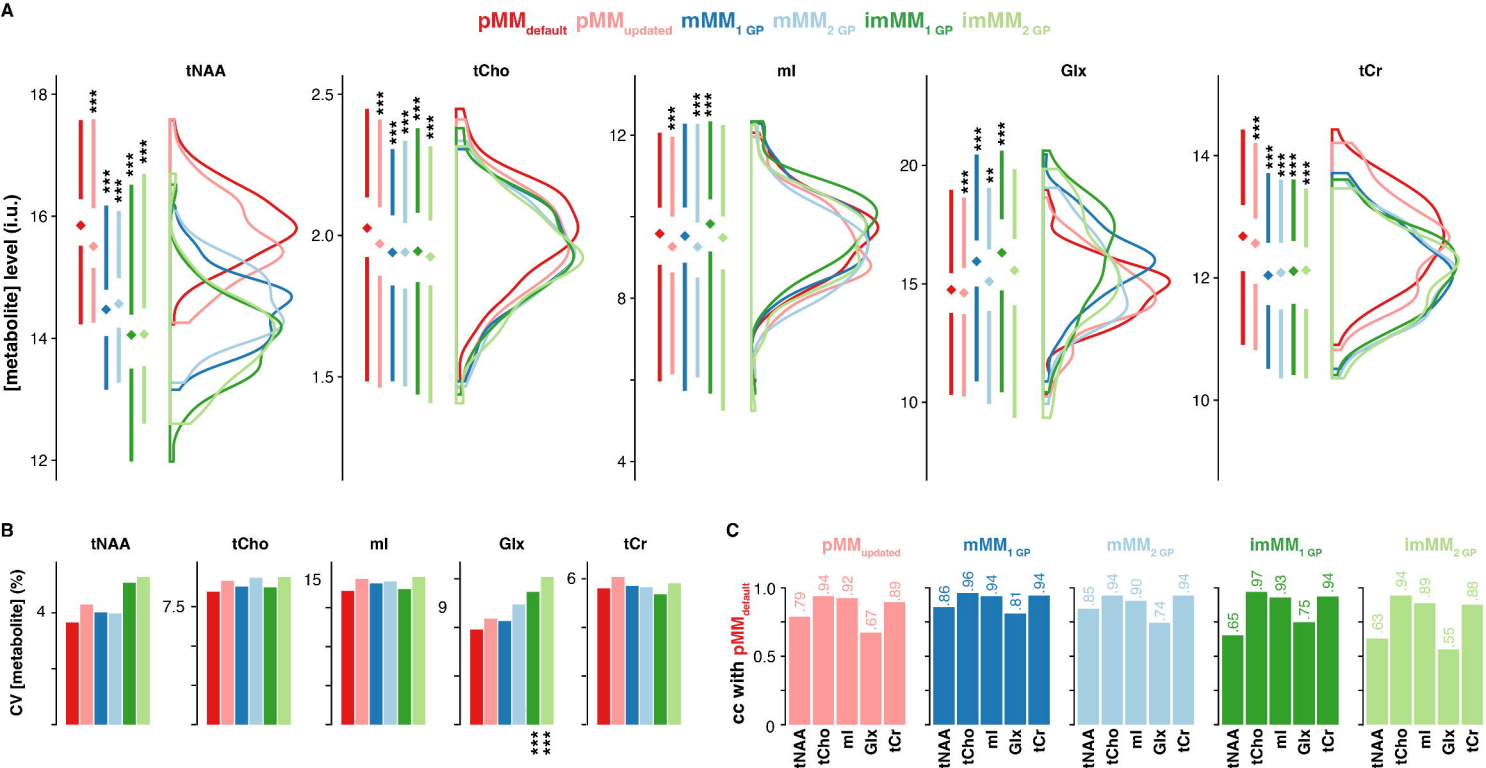
A
pMM default
pMM updated
mMM 1 GP
mMM 2 GP
imMM 1 GP
imMM 2 GP
tNAA
tCho
mI
Glx
tCr
[metabolite] level (i.u.)
B
CV [metabolite] (%)
C
cc with pMM default
.79 .94 .92 .67 .89
.86 .96 .94 .81 .94
.85 .94 .90 .74 .94
.65 .97 .93 .75 .94
.63 .94 .89 .55 .88

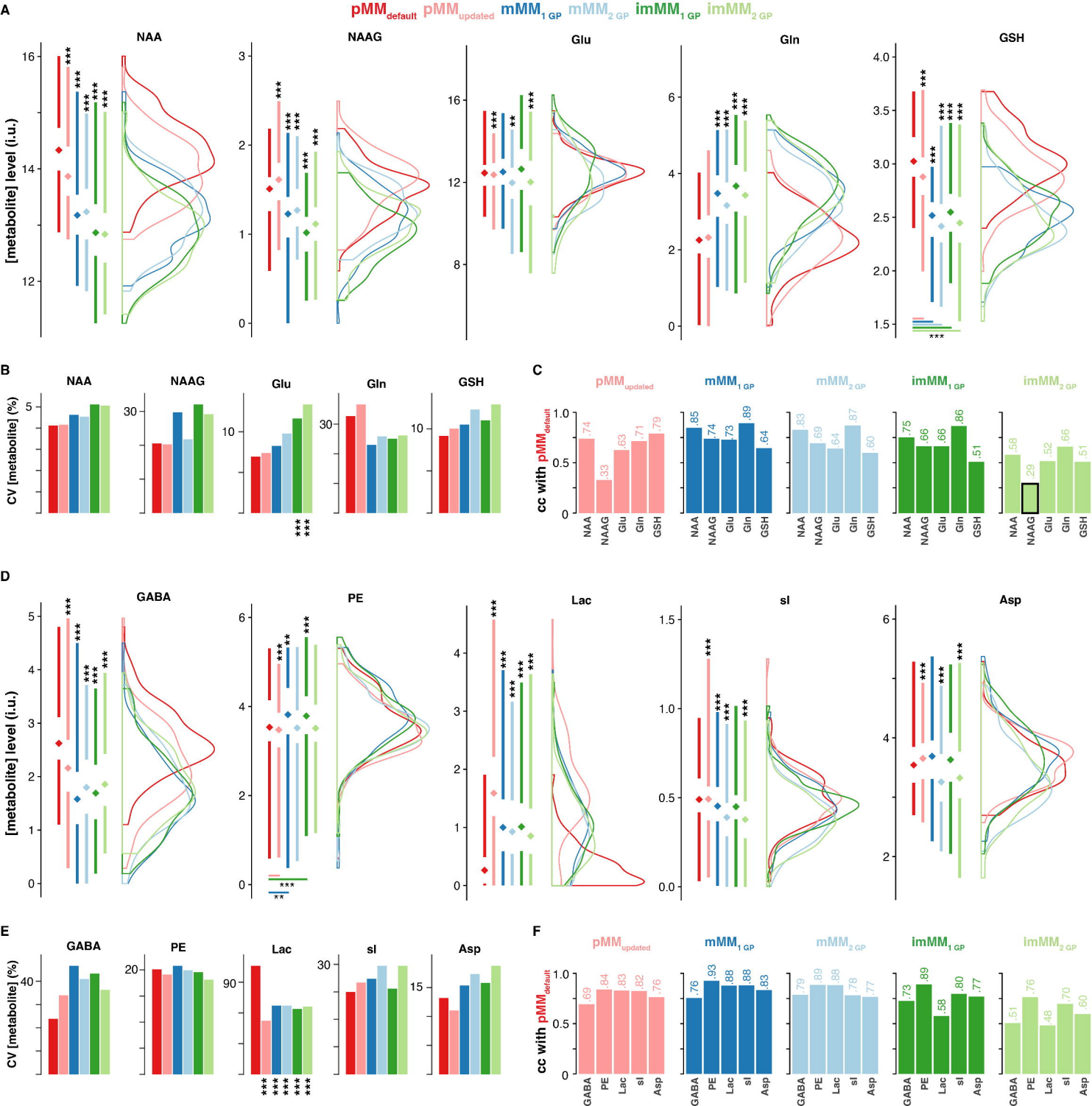
pMM default
pMM updated
mMM 1 GP
mMM 2 GP
imMM 1 GP
imMM 2 GP
A
NAA
NAAG
Glu
Gln
GSH
[metabolite] level (i.u.)
B
CV [metabolite] (%)
C
cc with pMM default
D
GABA
PE
Lac
sI
Asp
E
F

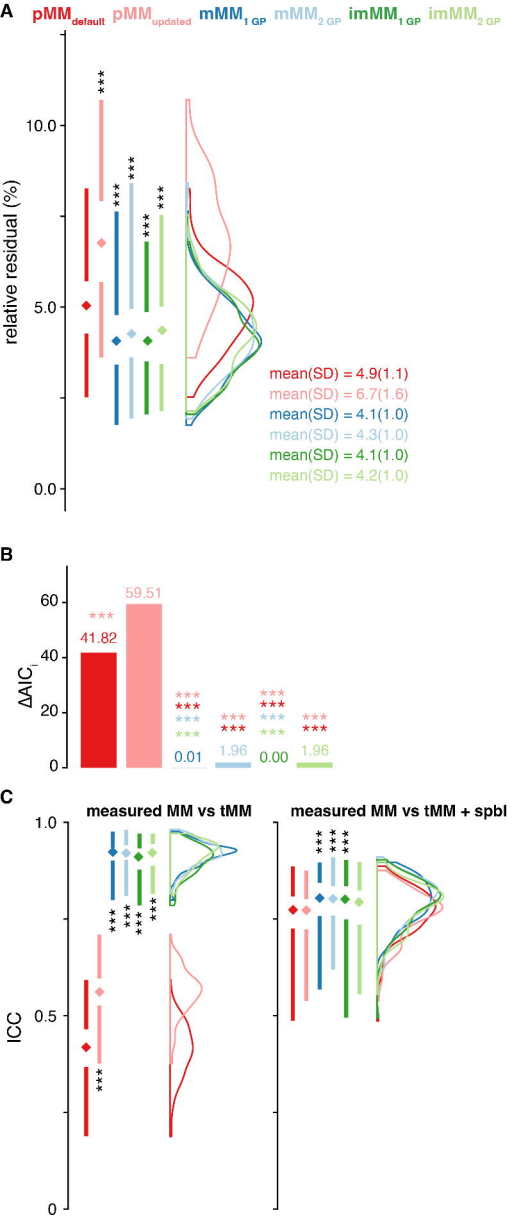
A
pMM default
pMM updated
mMM 1 GP
mMM 2 GP
imMM 1 GP
imMM 2 GP
relative residual (%)
10.0
5.0
0.0
***
mean(SD) = 4.9(1.1)
mean(SD) = 6.7(1.6)
mean(SD) = 4.1(1.0)
mean(SD) = 4.3(1.0)
mean(SD) = 4.1(1.0)
mean(SD) = 4.2(1.0)
B
ΔAIC i
60
40
20
0
41.82
59.51
0.01
1.96
0.00
1.96
C
measured MM vs tMM
measured MM vs tMM + spbl
ICC
1.0
0.5
0

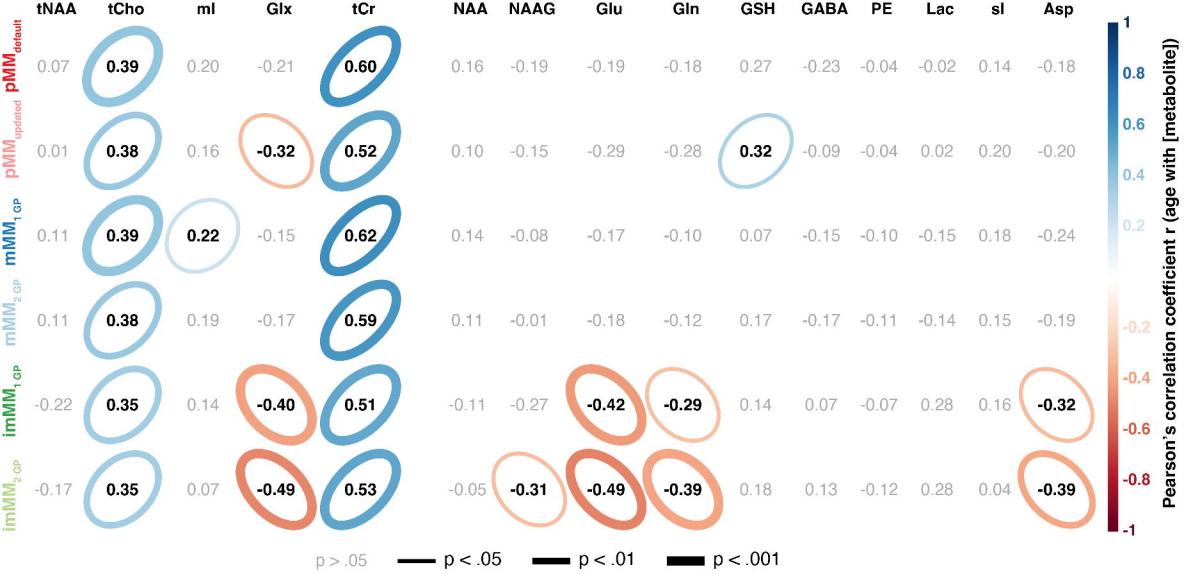
tNAA tCho mI Glx tCr NAA NAAG Glu Gln GSH GABA PE Lac sI Asp
pMM default
0.07 0.39 0.20 -0.21 0.60 0.16 -0.19 -0.19 -0.18 0.27 -0.23 -0.04 -0.02 0.14 -0.18
pMM updated
0.01 0.38 0.16 -0.32 0.52 0.10 -0.15 -0.29 -0.28 0.32 -0.09 -0.04 0.02 0.20 -0.20
mMM 1 GP
0.11 0.39 0.22 -0.15 0.62 0.14 -0.08 -0.17 -0.10 0.07 -0.15 -0.10 -0.15 0.18 -0.24
mMM 2 GP
0.11 0.38 0.19 -0.17 0.59 0.11 -0.01 -0.18 -0.12 0.17 -0.17 -0.11 -0.14 0.15 -0.19
imMM 1 GP
-0.22 0.35 0.14 -0.40 0.51 -0.11 -0.27 -0.42 -0.29 0.14 0.07 -0.07 0.28 0.16 -0.32
imMM 2 GP
-0.17 0.35 0.07 -0.49 0.53 -0.05 -0.31 -0.49 -0.39 0.18 0.13 -0.12 0.28 0.04 -0.39
1 0.8 0.6 0.4 0.2 -0.2 -0.4 -0.6 -0.8 -1
Pearson's correlation coefficient r (age with [metabolite])
p > .05 p < .05 p < .01 p < .001

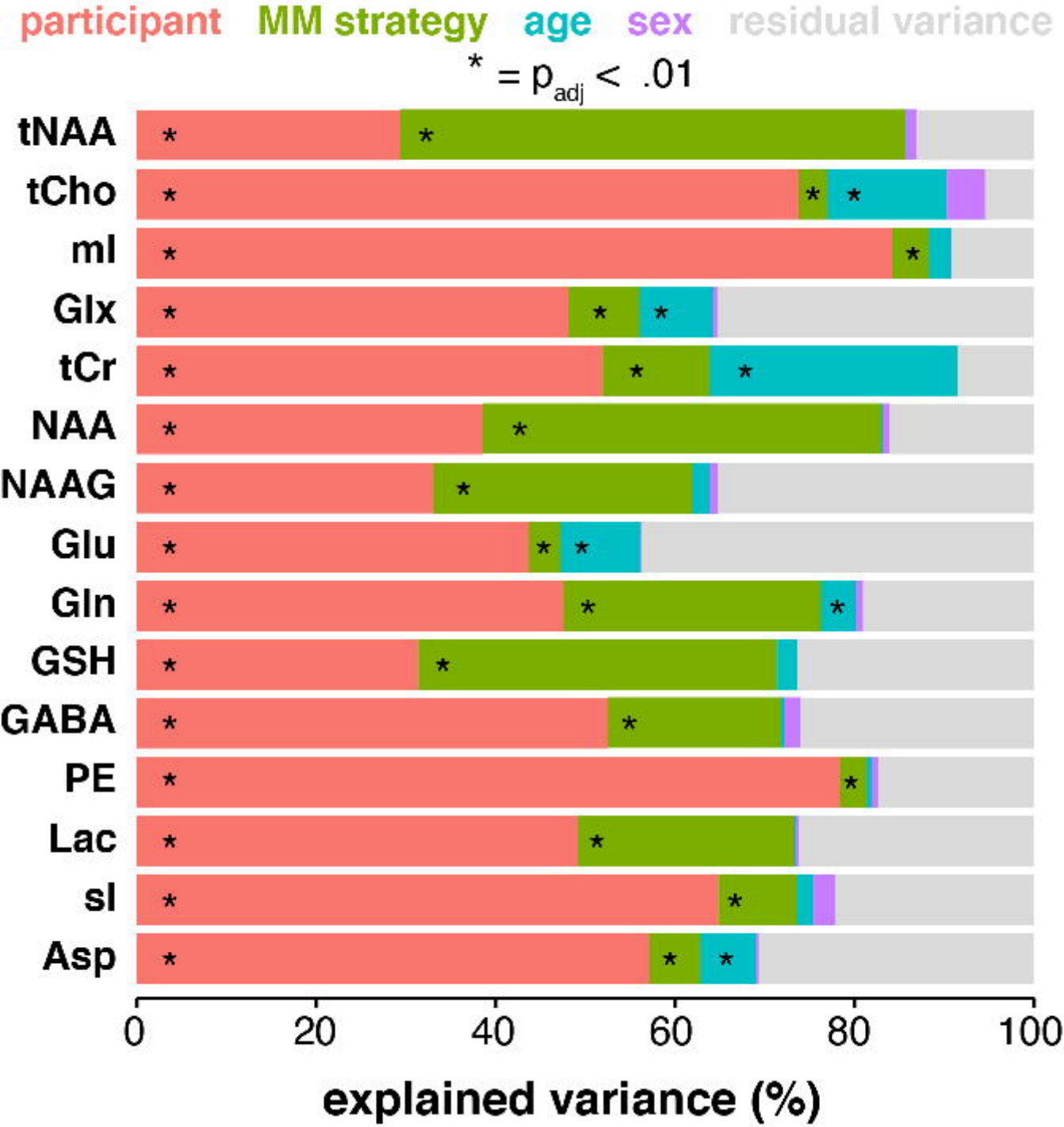
participant
MM strategy
age
sex
residual variance
* = p_adj < .01
tNAA
tCho
mI
Glx
tCr
NAA
NAAG
Glu
Gln
GSH
GABA
PE
Lac
sI
Asp
0
20
40
60
80
100
explained variance (%)

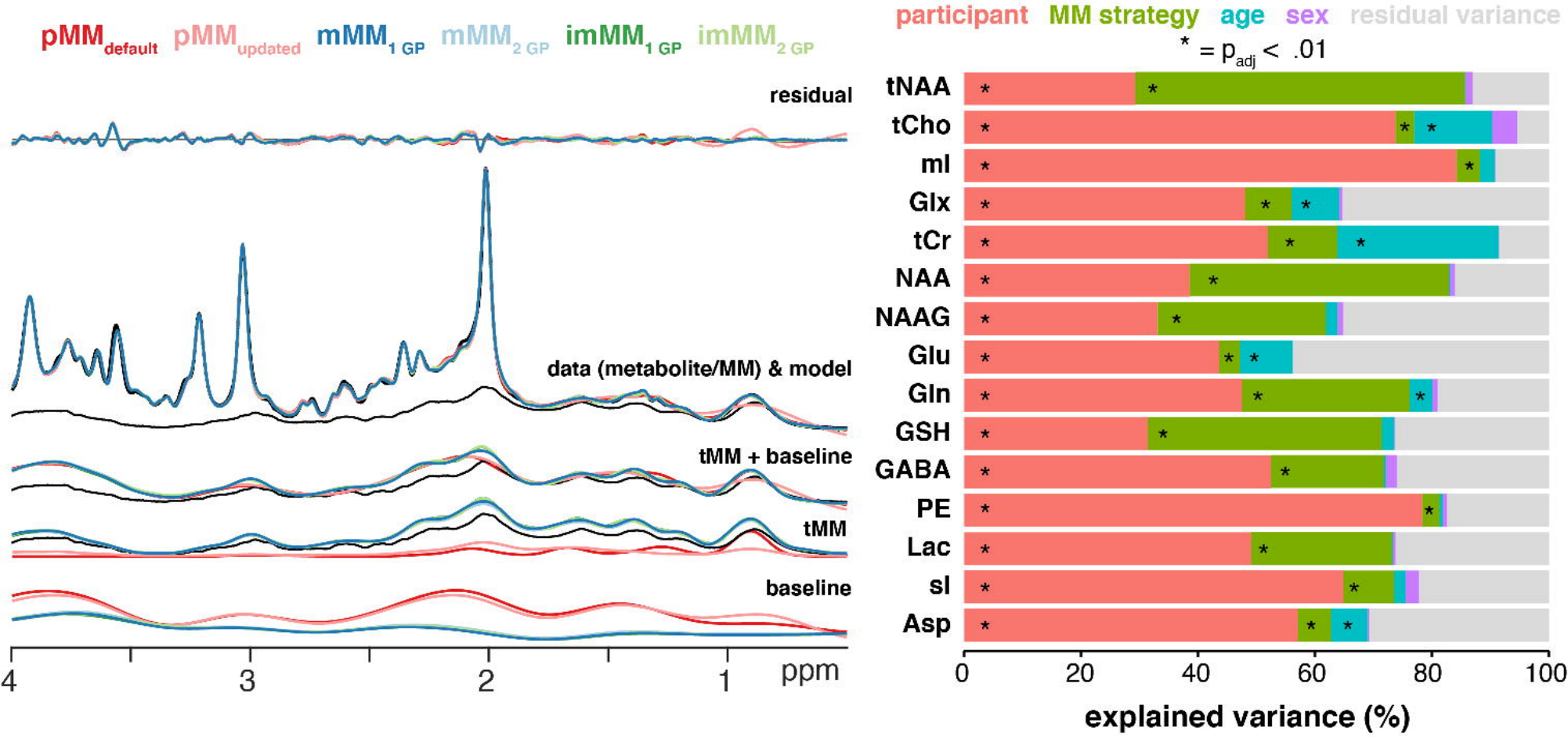
pMM default
pMM updated
mMM 1 GP
mMM 2 GP
imMM 1 GP
imMM 2 GP
residual
data (metabolite/MM) & model
tMM + baseline
tMM
baseline
4
3
2
1
ppm
participant
MM strategy
age
sex
residual variance
* = p adj < .01
tNAA
tCho
mI
Glx
tCr
NAA
NAAG
Glu
Gln
GSH
GABA
PE
Lac
sI
Asp
0
20
40
60
80
100
explained variance (%)